Chin. J. Astron. Astrophys. Vol. 2 (2002), No. 6, 501–524
( http://www.chjaa.org or http://chjaa.bao.ac.cn )

Chinese Journal of Astronomy and Astrophysics

# Properties of Broad Band Continuum of Narrow Line Seyfert 1 Galaxies

Hong-Yan Zhou ⋆ and Ting-Gui Wang
Center for Astrophysics, University of Science and Technology of China, Hefei 230026
National Astronomical Observatories, Chinese Academic of Science, Beijing 100012

Received 2002 May 18; accepted 2002 September 23

**Abstract** We have performed a statistical study of the properties of the broad band continuum of Narrow Line Seyfert 1 galaxies (NLS1s) by collecting ratio, infrared, optical and X-ray continuum data from various databases and compared the results with control samples of Broad Line Seyfert 1 galaxies (BLS1s). We find that the fraction ($\sim 6\%$) of Radio Loud (RL) NLS1s is significantly less than that of BLS1s ($\sim 13\%$), which is caused by the lack of radio-very-loud sources in the former. The rarity of RL NLS1s, especially radio-very-loud ones, is consistent with the scenario of small black hole and high accretion rate for NLS1s. Six new radio loud NLS1s are found and five RL NLS1 candidates are presented. In comparison with the BLS1s, the NLS1s tend to have stronger far infrared emission, cooler infrared colors and redder $B-K$ color, which suggests that NLS1s are hosted by dust-richer nuclei. The NLS1s also show steeper soft X-ray spectrum and large soft X-ray to optical flux ratio, while a significant fraction show flat soft X-ray spectra. At least two factors can account for this, absorption and spectral variability. We also perform a correlation analysis between various broad band data. It is found that most correlations identified for NLS1s are also valid for radio quiet BLS1s: (1) the optical colors are anti-correlated with X-ray spectral index; (2) higher optical, X-ray and NIR luminosity objects show bluer optical colors and red $H-K$ color; (3) higher luminosity objects show warmer IRAS color; (4) the radio loudness correlates with $B-K$ and X-ray to optical flux ratio. Radio loud objects behave somewhat differently in a few correlations.

**Key words:** galaxies: active — galaxies: Seyfert — radiation: continuum

## 1 INTRODUCTION

Narrow Line Seyfert 1 Galaxy (NLS1) has been one of the hot topics of the AGN research in recent years. The formal spectral classification criteria (Pogge 2000) are:

⋆ E-mail: mtzhou@mail.ustc.edu.cn

- Narrow permitted lines only slightly broader than the forbidden lines.
- [OIII]/H$\beta$ $< 3$, but exceptions are allowed if there is a strong [FeVII] and [FeX] present, unlike what is seen in Seyfert 2 galaxies.
- FWHM (H$\beta$) $< 2000\,\mathrm{km\ s^{-1}}$.

NLS1s usually also show strong permitted FeII emission line in the optical and ultraviolet bands. Other extreme properties of NLS1s have been revealed by X-ray and ultraviolet observations: steep soft X-ray spectrum, rapid variability, dense line emitting gas and commonly blue shifted UV line profile (Boller, Brandt & Fink 1996; Leighly 1999; Aoki & Yoshida 1999; Wills et al. 1999; Leighly 2000). In fact, these extreme properties are the extension, at the extreme, of the set of correlations of various observables with the H$\beta$ line width (Boroson & Green 1992; Laor et al. 1994; Wang, Brinkmann & Bergeron 1996), that narrower lines are correlated with steeper X-ray spectra, stronger H$\beta$ blue wings, faster X-ray variations, stronger optical FeII emission, weaker [OIII] emission, and denser BLR clouds. These form the so-called principal component 1 (PC1) (Boroson & Green 1992, hereafter BG92). However, there is still controversy whether some of the correlations should be included in the PC1, e.g., Veron-Cetty, Veron & Goncalves (2001) found that NLS1s do not show systematically weaker [OIII ] strengths.

The physical driver of PC1 is not yet clear. It was proposed that the PC1 is related either to the fundamental parameters of the black hole accretion disk model, such as the black hole mass and accretion rate, or geometrical effect such as the viewing angle (BG92; Boller et al. 1996; Wang et al. 1996; Laor et al. 1997; Tanigucchi et al. 2001; Sulentic et al. 2000; Marziani et al. 2001). However, no single model is able to reproduce all the correlations. This is partly due to our ignorance of detailed physical processes and their relations to fundamental parameters, such as the formation of BLR clouds, FeII lines and soft X-ray spectrum. The viewing-angle picture seems relatively simple, but the lack of information on the effect of the viewing angle on the spectrum make this model hard to be tested. Despite these difficulties, since the NLS1s lie at the extreme negative end of the PC1, they may well have extreme values of some primary physical parameter; hence their usefulness for constraining models.

Though the emission line and X-ray properties of NLS1s are extensively studied in past years, relatively little work has been done on their broad-band continuum properties. In the radio band, Ulvested et al. (1995) carried out high resolution VLA radio observations of a small sample of NLS1s, and tentatively concluded that NLS1s do not differ noticeably from nearby classical Type 1 and Type 2 Seyfert galaxies at centimeter wavelengths, in contrast to their remarkably different properties in the X-ray continuum. With the increased database of NLS1 since then, and with the many NLS1s detected by the radio survey, this issue certainly needs to be re-examined. While, until recently, NLS1s were known as radio quiet AGNs, the past two years saw the report of three Radio-Loud (RL) NLS1s (Siebert et al. 1999; Grupe et al. 2000). Their typical radio loudness (defined as $R = \log(f_{5\,\mathrm{GHz}}/f_{\mathrm{opt}})$) are all less than 2, so they are less powerful than the classical radio sources. Their radio spectra can be either steep or flat. The nature of radio sources in RL NLS1s is of particular interest in view of their distinct properties– the RL NLS1s show extreme characteristics opposite to a typical RL AGNs, e.g., extremely steep soft X-ray spectrum in NLS1 versus usually flat spectrum in a RL AGN, very weak [OIII ] emission in NLS1s versus strong [OIII ] emission in a RL object (Sulentic et al. 2000). These differences, together with the occurrence of radio-loud sources in Seyfert 1 and NLS1s, are certainly worthy of further studies.

As in the radio band, NLS1s are not well studied in the middle and near infrared bands, and contradictory results appear in the literature. On one hand, IRAS selected Seyfert galaxies contain a high fraction of NLS1s. On the other hand, in a soft X-ray-selected sample, Grupe et al. (1999) did not find any systematic difference in the optical-to-infrared flux ratio between NLS1s and normal Seyfert 1 galaxies. Further study on this issue is certainly needed. Even less work has been done in the near infrared than in the mid-infrared.

In this paper, we collect radio, infrared, optical and X-ray continuum data from various databases, and carry out a statistical study of the broad band continuum properties of the NLS1s. The paper is organized as follows: Section 2 describes the samples of NLS1s and BLS1s, and the data used in this paper. In Section 3, we perform a statistical analysis for the samples and present the main results. Section 4 gives our preliminary conclusions. Throughout this paper, we assume a Hubble's constant $H_0 = 50$ km s$^{-1}$ Mpc$^{-1}$, and $q_0 = 0.5$.

## 2 THE SAMPLE AND DATA

### 2.1 The NLS1 Sample and the Comparison BLS1 Sample

We took all the 205 NLS1s from Tables 1 and 3 of the Veron-Cetty & Veron (2001, hereafter VV01) catalog, for three of them (IRAS 06269−0543, IRAS 09426+1929, and IRAS 16075+2838) no optical magnitudes were listed. We looked their $F$ and $B_J$ magnitudes in the GSC 2.2.01 and set $V = 0.5(F + B_J)$ as their approximate $V$ magnitudes. Of all the 205 NLS1s, the optical magnitudes for 21 objects listed in VV01 are "O-magnitudes", and three are photo-magnitudes (marked with "O" and "*" in Table 1, respectively). For convenience of our analysis, we calculated the $AB$-magnitudes at 0.55 $\mu$m for these 23 sources, assuming an average optical spectral index of $\alpha_{\rm opt} = 0.5$. The $AB$-magnitude is defined as $AB(\lambda) = -2.5 \times \log(f_\nu(\lambda)) + 16.37$ (mag), where $f_\nu(\lambda)$ is flux density in mJy at wavelength $\lambda$. All optical magnitudes used in the present paper have been corrected for the Galactic reddening assuming $A(V) = 3.1E(B-V)$. Starting from this initial NLS1 sample, we searched for their counterparts in the radio (NVSS/FIRST), far/middle-IR (IRAS FSC), near-IR, and soft X-ray (ROSAT) bands. The data used in this paper are listed in Table 1 and will be described in the rest of this section.

**Table 1** Broad Band Data of NLS1s[†]

| ID | Common Name | Mag | $z$ | $f_{6\,\rm cm}$ | $f_{20\,\rm cm}$ | $f_{100\mu\rm m}$ | $f_{60\mu\rm m}$ | $f_{25\mu\rm m}$ | $f_{12\mu\rm m}$ | $K_s$ | $H$ |
|---|---|---|---|---|---|---|---|---|---|---|---|
| | | | | mJy | mJy | mJy | mJy | mJy | mJy | mag | mag |
| 1 | RXS J00001+0523 | –20.5 | 0.04 | ··· | ··· | ··· | ··· | ··· | ··· | ··· | ··· |
| 2 | RXS J00201+3244 | –21.5 | 0.082 | ··· | ··· | ··· | ··· | ··· | ··· | 13.563±0.054 | 14.387±0.062 |
| 3 | RXS J00247+0820 | –20.8 | 0.067 | ··· | ··· | ··· | ··· | ··· | ··· | ··· | ··· |
| 4 | RXS J00323+2423 | –20.7 | 0.066 | ··· | ··· | ··· | ··· | ··· | ··· | 14.202±0.065 | 14.531±0.062 |
| 5 | WPVS 7 | –20.4 | 0.029 | ··· | ··· | ··· | ··· | ··· | ··· | ··· | ··· |
| 6 | MARK 957 | –22.3 | 0.073 | ··· | 16.24 | 3207 | 2095 | 245 | <188.2 | 12.541±0.050 | 13.413±0.055 |
| 7 | 2E 0039–0158 | –24.2 | 0.35 | ··· | ··· | ··· | ··· | ··· | ··· | 14.996±0.119 | 15.954±0.145 |
| 8 | RXS J00444–2616 | –20.8 | 0.061 | ··· | ··· | ··· | ··· | ··· | ··· | ··· | ··· |
| 9 | RXS J00449+1921 | –23.2 | 0.181 | 7 | ··· | <815.6 | 321.6 | <182.2 | <137.2 | ··· | ··· |
| ⋮ | | | | | | | | | | | |
| 205 | IRAS 23410+0228 | –20.9 | 0.091 | ··· | 5.74 | 2199 | 2280 | 447 | <153 | ··· | ··· |

**Table 1 Continued**

| Common Name | $J$ | $F$ | $V$ | $B_J$ | $F_{\rm x}$ [a] | $\Gamma^{\rm G}$ | $N_{\rm H}^{\rm G}$ [b] | $\Gamma^{\rm F}$ | $N_{\rm H}^{\rm F}$ [b] |
|---|---|---|---|---|---|---|---|---|---|
| | mag | mag | mag | mag | | | | | |
| RXS J00001+0523 | ··· | 15.24±0.42 | 16.4 | 16.12±0.42 | 37.59 | $2.98^{+0.17}_{-0.17}$ | 5.08 | $3.08^{+1.15}_{-1.07}$ | $5.41^{+3.70}_{-3.10}$ |
| RXS J00201+3244 | 15.145±0.061 | 14.95±0.42 | 17 | 16.08±0.42 | 9.11 | $2.59^{+0.36}_{-0.44}$ | 5.64 | $2.76^{+2.18}_{-1.98}$ | $6.33^{+9.30}_{-5.90}$ |
| RXS J00247+0820 | ··· | 15.50±0.43 | 17.2 | 16.48±0.42 | 11.6 | $3.37^{+0.53}_{-0.48}$ | 4.79 | ··· | ··· |
| RXS J00323+2423 | 15.349±0.056 | 15.54±0.36 | 17.3 | 17.12±0.36 | 6.11 | $2.25^{+0.31}_{-0.33}$ | 3.39 | $4.40^{+>1.55}_{-2.21}$ | $10.66^{+>9.60}_{-7.20}$ |
| WPVS 7 | ··· | ··· | 15.28 | ··· | ··· | ··· | 2.55 | ··· | ··· |
| MARK 957 | 14.130±0.069 | 11.87±0.43 | 15.14 | 12.43±0.41 | 7.57 | $2.21^{+0.07}_{-0.04}$ | 6.18 | $3.28^{+0.26}_{-0.19}$ | $12.33^{+1.70}_{-1.60}$ |
| 2E 0039–0158 | 16.445±0.094 | 16.77±0.43 | O17.5 | 17.34±0.42 | ··· | ··· | 4.03 | ··· | ··· |
| RXS J00444–2616 | ··· | ··· | 17 | ··· | 1.24 | $2.08^{+0.16}_{-0.15}$ | 1.36 | ··· | ··· |
| RXS J00449+1921 | ··· | 16.14±0.42 | O17 | 16.58±0.43 | 22.5 | $3.26^{+0.23}_{-0.22}$ | 3.67 | $3.97^{+>1.95}_{-1.69}$ | $5.80^{+>6.20}_{-4.40}$ |
| ⋮ | | | | | | | | | |
| IRAS 23410+0228 | ··· | 14.93±0.41 | 17.8 | 16.14±0.40 | 10.06 | $3.24^{+0.44}_{-0.43}$ | 4.86 | ··· | ··· |

[a] in units of $10^{-12}$ erg cm$^{-2}$ s$^{-1}$. [b] $n$ units of $10^{20}$ cm$^{-2}$.

† For the full content of Table 1 see 'www.chjaa.org' or 'chjaa.bao.ac.cn'

In order to compare our results with normal Seyfert 1 galaxies, a comparison sample of BLS1s was also compiled. There are 3236 Sy1(=S1+S1.0+S1.2+S1.5) in VV01 after removing the objects with classifications S1.8 or S1.9, which probably suffer large dust reddening. The VV01 catalog does not distinguish radio galaxies from Seyfert 1 galaxies, therefore, Seyfert 1 galaxies are just broad line AGNs. Following their classification, we simply call these objects BLS1s. This sample forms the parent sample of our comparison BLS1 sample. Certainly some of these sources may actually be NLS1s for the lack of a good quality spectrum. However, as NLS1s account for only a small part of Seyfert 1 galaxies, this will not introduce serious confusion. Control subsamples drawn from this parent one are described in a later section.

### 2.2 Data at other Bands

The radio data are mainly from three sources: 6 cm and 11 cm from VV01 itself, 1.4 GHz ($\sim$ 20 cm) from NVSS and FIRST. In order to include possibly extended radio sources, we searched for NVSS and FIRST counterparts within 20 arcsec for both samples. We found 64 and 489 NVSS counterparts for 182 NLS1s and 2556 BLS1s within the NVSS area coverage. Because the survey limit of FIRST is about 2 times deeper than NVSS, and the sky area covered by FIRST is also covered by NVSS, we cross-correlated FIRST and our N/BLS1 samples to enlarge our radio-selected subsamples. In this matching, chance coincidences are estimated to be less than 1%. There are 43 NLS1s detected by FIRST, out of which three NLS1s (MARK 739 E, RXS J16446+2613, and RXS J09571+2433) have two FIRST counterparts, and 19 NLS1s are not detected by NVSS. Two NVSS counterparts of 2 E 1640+5345 are separated by about 10 arcsec. The FIRST image reveals an associated object, maybe a core-jet structure (see Figure 1). As comparison, 736 of the 3626 BLS1s have NVSS counterparts within 20 arcsec and five of them are probably double radio sources. 431 BLS1s were detected in FIRST, out of which 59 have two FIRST counterparts each and 157 are not detected by NVSS. For sources with multiple radio counterparts, the radio flux of the nearest one is used in the rest of this paper. This is justified given the accuracy of the radio and optical positions. For the sources detected both by NVSS and FIRST, the FIRST flux is adopted. In fact, NVSS and FIRST fluxes are

consistent in most cases.

The only comprehensive all sky survey available in the far/middle-IR so far was done by the Infrared Astronomical Satellite (IRAS). In this paper, we make use of the IRAS Faint Source Catalog (IRAS FSC), $|b| > 10$, Version 2.0 (Moshir et al. 1989), as most of the objects in our samples are relatively faint. Based on a matching of the IRAS FSC sources with our N/BLS1 samples ($separation \leq 1$ arcmin) , we found 64 and 361 IRAS counterparts for 205 NLS1s and 3626 BLS1s, respectively. Chance coincidences are expected to be 1 for the NLS1s and 15 for the BLS1s. Also, when two counterparts were found for one source, we choose the nearer one and take it as the real match.

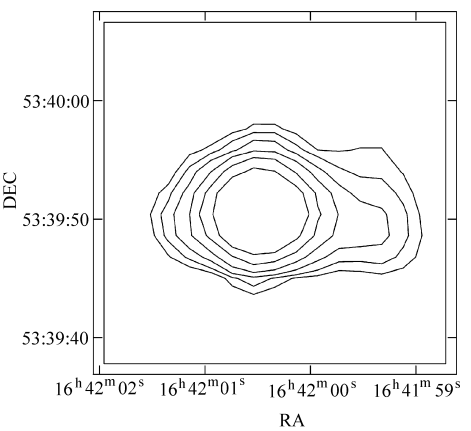


Fig. 1 Radio (FIRST) image of RXS J16526+4417 shows a possible jet-like structure.

We searched for unresolved 2MASS (The 2 Micron All Sky Survey, Skrutskie et al. 1997) counterparts for both of our samples within 5 arcsec and found 111 counterparts for the NLS1s and 987 for the BLS1s, respectively. The initial errors on the 2MASS astrometry are on average 0.3 arcsec, so the uncertainty in the astrometric matching is dominated by the errors on the coordinates of the Seyfert 1 galaxies. There are 159 NLS1s that have optical positions accurate to $\lesssim 1$ arcsec (denoted "O" by VV01), and the remaining 40 NLS1s have positions that should be better than a few arcsecs. The position accuracies of BLS1s are similar to NLS1s. In the above matching, each of the two sources in our NLS1 sample (B3 1702+457 and RX J14517+5241) has two counterparts, while about 30 objects in the BLS1 sample have multiple 2MASS counterparts. With the assumption that the 2MASS sources are distributed randomly on the sky, we expect that the number of chance matching is 2 and 26 for NLS1s and BLS1s (considering the half sky coverage of the Second Incremental Release), respectively. Therefore we expect that most of these double sources are chance coincidences instead of real physical associations. For those sources with more than one 2MASS counterparts, we choose the nearest one and take it as the real match.

We searched the ROSAT All Sky Survey Bright Source Catalog (RBSC) (Voges et al. 1999) and the ROSAT Source Catalog of pointed observations (RSC) (Voges et al. 1997) for soft-X-ray counterpart of the NLS1s and BLS1s. The cross-correlations of the ROSAT catalogs with our BLS1s and NLS1s yielded 271 and 1785 counterparts within 1 arcmin of the optical positions. Some of these are the same object observed several times, while others are different

X-ray sources. To distinguish these two possibilities, we used also the observing dates in the catalogs. For objects with several X-ray counterparts within the same observation, we chose the nearest one, and for objects with multiple ROSAT observations, we chose the one with the longest exposure time. Finally, we had the X-ray data for 161 NLS1s and 1346 BLS1s.

Although in a few cases, a simple power law model is not a satisfactory description of the spectrum for the whole ROSAT band (0.1–2.4 keV), the photon index $\Gamma$ (defined as $f_\nu \propto \nu^{-\Gamma+1}$) can serve as a useful quantitative measure of its steepness. Following Schartel et al. (1996) and Yuan et al. (1998), we calculated the X-ray photon-index and X-ray flux by fitting the 2 hardness ratios and the count-rate given in the ROSAT catalogs by assuming a Galactic absorption column density ($N_{\rm H}^{\rm G}$). This photon index is denoted as $\Gamma \equiv \Gamma^{\rm G}$. Since Seyfert 1 galaxies usually do not show strong absorption over the Galactic column density in the soft X-ray band (e.g., Walter & Fink 1993; Boller, Brandt & Fink 1996; Wang, Brinkmann & Bergeron 1996), this photon index will be used in most of the statistical analysis presented below. We also made a fit of the free absorption column to the hardness ratio in order to constrain the intrinsic absorption column density for objects with sufficient counts (the free fitting photon index is denoted as $\Gamma^{\rm F}$ and the corresponding column density as $N_{\rm H}^{\rm F}$).

### 2.3 The limitations of the sample

All of the types of AGNs listed in the V&V catalog are neither complete nor uniform in any sense, hence care must be taken in any statistical analysis, especially when making comparisons between samples. While most of the sources in our NLS1 sample are discovered in the X-ray survey, a majority of the BLS1s are optically selected. So when comparisons were made between NLs1s and BLS1s, we actually used subsamples selected from the BLS1 parent sample with a similar distribution of optical magnitude and luminosity. Hence, we can safely believe that the optical photometric properties of the two are alike. The broad band continuum properties of NLS1s and BLS1s and the differences between the two can be expected to provide clues for future research.

## 3 STATISTICAL RESULTS

In this section, we will present a statistical study of the broad band continuum. We shall call a test "statistically significant" if the chance probability ($P_r$) is less than 1%, and "marginally significant" if the chance probability is $1\% < P_r < 5\%$.

### 3.1 Radio Properties

In our NLS1 sample 182 sources are located north of $-40$ degree (the area covered by NVSS), and 63 of these were detected in the NVSS (detection rate $\simeq$ 34.6%). As a measure of radio loudness, we calculated the logarithmic ratio, $R_{\rm eff}$, of the radio 6 cm flux density to the flux density at 2500Å ($R_{\rm eff} \equiv \log(f_{6\,\rm cm}/f_{2500\mathring{\rm A}})$), where $f_{6\,\rm cm}$ is calculated from $f_{20\,\rm cm}$ and $f_{2500\mathring{\rm A}}$ is calculated from $V$-magnitude, assuming that the optical and radio spectral indexes are both 0.5. It was found that 11 NLS1s ($\sim$ 6.0% ) detected by NVSS are radio loud, i.e., with $R_{\rm eff} > 1$. For comparison, 736 out of the 3028 BLS1s northern of $-40$ degree were detected by NVSS (5 BLS1s probably have double radio counterparts), at a detection rate $\simeq$ 23.9%. We also calculated their $R_{\rm eff}$ (10 of the 736 sources have no optical photometric data listed in VV01) and found that 450 BLS1s have $R_{\rm eff} > 1$ ($\sim$ 14.9%). The proportion of radio-loud objects of BLS1s is significantly larger than that of NLS1s, at a chance probability of 0.2% ($\chi^2 = 9.3$).

Comparing NLS1 with the parent sample of BLS1 may suffer from selection effects. In particular, the detection rate depends on the distribution of optical magnitude, and the radio loudness might also depend on the optical luminosity. Therefore, we select a comparison BLS1 sample of size $3 \times 182$ on the sky north of $-40$ degree from the parent BLS1 sample by a one-to-one matching of the $V$ magnitude ($\Delta V < 0.2^{\rm m}$) and redshift of each BLS1 with NLS1, and with a difference in $z$ is as small as possible (Figure 2). We find that 190 of these 546 BLS1s have NVSS counterparts within 20 arcsec (detection rate $\simeq 34.8\%$), similar to NLS1s. However, the proportion of radio loud BLS1s is relatively larger than that of NLS1s—69 BLS1s ($\sim 12.6\%$) with $R_{\rm eff} > 1$—at a chance probability of 2% ($\chi^2 = 5.4$). The difference is due to the lack of "radio very loud" (i.e., $R_{\rm eff} > 2.5$) NLS1s. In fact, radio very loud objects account for about 7% in the BLS1s, but none in the NLS1s. The difference is statistically significant at a chance probability of 0.2% according to the $\chi^2$ test. Similar difference is seen in the 20 cm power distribution: powerful radio sources ($P_{20\,\rm cm} > 10^{25.1}$ W s$^{-1}$) are not present in the NLS1s (Figure 3). The mean radio-loudness and radio power are $\langle R_{\rm eff}\rangle_{\rm BLS1} = 0.53 \pm 0.06$ and $\langle \log P_{20\,\rm cm}\rangle_{\rm BLS1} = 23.17 \pm 0.07$ W Hz$^{-1}$, for the control BLS1 sample (after ignoring the radio-very-loud ones); $\langle R_{\rm eff}\rangle_{\rm NLS1} = 0.42 \pm 0.10$, and $\langle \log P_{20\,\rm cm}\rangle_{\rm NLS1} = 23.21 \pm 0.11$ W Hz$^{-1}$ for the NLS1 sample.

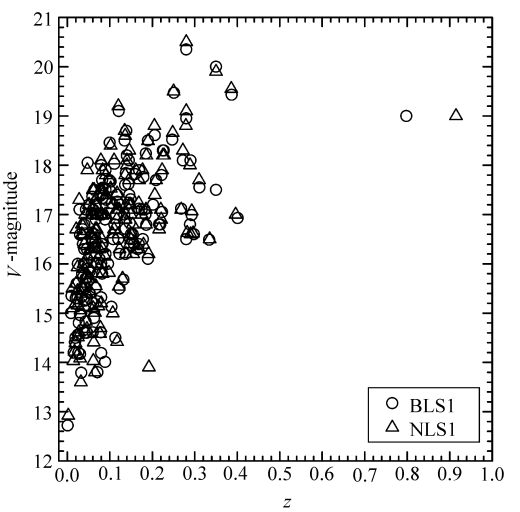


Fig. 2 $V$-magnitude versus redshift $z$ diagram of for NLS1s and control sample of BLS1s (only one match for each object is shown). Note the one-to-one match of the optical magnitude and redshift for the two samples.

Using the 6 cm radio fluxes listed in VV01 and the 20 cm fluxes in NVSS, we calculated the radio-loudness $R_{6\,\rm cm}$ or $R_{\rm eff}$ for 71 NLS1s with available data. We find 9 RL NLS1s with $R_{6\,\rm cm} > 1$ in our NLS1 sample, out of which three (RXS J00449+1921, PKS 0558–504 and HE 0132–4313) were previously known (Siebert et al. 1999; Gliozzi et al. 2000; Grupe et al. 2000). They are listed in Table 2. Table 3 lists another five candidates of radio-loud NLS1 with $R_{\rm eff} > 1$. Some of these RL NLS1 candidates in Table 3 should be radio-loud though further observations at 6 cm are needed. All of the three powerful RL NLS1 (2E 1640+5345,

RXS J16290+4007, and RX J16446+2619) have very flat radio spectra with spectral indexes $\alpha_{6-20\,\mathrm{cm}} = -0.24,\ -0.78$, and 0.01, respectively. Grupe et al. (2000) noticed that the quoted steep radio spectrum of HE 0132–4313 may be due to the variability of the radio source and the spectral index was calculated using non-simultaneous observations. The mean spectral index of the 16 NLS1s with 20 cm and 6 cm observations are $\langle\alpha_{6-20\,\mathrm{cm}}\rangle = 0.74 \pm 0.19$, significantly steeper than the average for the control sample of BLS1s, $\langle\alpha_{6-20\,\mathrm{cm}}\rangle = 0.10 \pm 0.10$. K-S test gives a chance probability of 0.3%. However, the 6 cm detections bias strongly toward the radio luminous objects, this result may be due to selection effect and should be treated with care.

**Table 2** 9 RL NLS1s from Veron-Cetty & Veron Catalog

| Common Name | $\log P_{20\,\mathrm{cm}}$ W·Hz$^{-1}$ | $\log P_{6\,\mathrm{cm}}$ W· Hz$^{-1}$ | $R_{20\,\mathrm{cm\,V}}$ | $R_{6\mathrm{cm}}$ | $\alpha_r$ [a] |
|---|---|---|---|---|---|
| 2E 1640+5345 | 24.47 | 24.60 | 2.15 | 2.45 | −0.24 |
| RXS J16290+4007 | 24.49 | 24.90 | 1.68 | 2.26 | –0.78 |
| HE 0132−4313 | | 25.13 | | 2.09 | 1.40[d] |
| RXS J16333+4718 | 24.62 | 24.46 | 2.01 | 2.02 | 0.30 |
| RXS J08066+7248 | 24.34 | 23.95 | 2.15 | 1.93 | 0.74 |
| PKS 0558−504 | | 25.00 | | 1.55 | 0.86[c] |
| RXS J00449+1921 | | 24.04 | | 1.08 | |
| B3 1702+457 | 24.30 | 23.64 | 1.52 | 1.03 | 1.26 |
| RXS J16446+2619[b] | 25.08 | 25.02 | 2.38 | 2.30 | 0.01 |

Notes: [a] Spectral index from 6 to 20 cm; [b] Radio flux at 6 cm is from Laurent-Muehleisen et al. (1997); [c] $\alpha_r$ c.f. Brinkmann et al. 1997; [d] $\alpha_r$ is calculated from 3.6 cm and 6 cm fluxes (data c.f. Group et al. 2000).

**Table 3** Basic Data for 5 Possible RL NLS1s

| Common Name | $\log P_{20\,\mathrm{cm}}$ W· Hz$^{-1}$ | $R_{\mathrm{eff}}$ | Sep (rad-opt) arcsec |
|---|---|---|---|
| IRAS 22453−1744 | 24.00 | 1.46 | 1.3 |
| IRAS 09426+1929 | 24.82 | 1.36 | 4.3 |
| IRAS 20181−2244 | 24.59 | 1.32 | 7.2 |
| IRAS 23410+0228 | 23.34 | 1.14 | 2.3 |
| RXS J15375+4943 | 23.74 | 1.12 | 1.0 |

### 3.2 Far/Mid-Infrared Properties

As mentioned in Section 2, 64 (or 31.2%) of the 205 NLS1s have IRAS FSC counterparts. For the 3236 BLS1s, only 361 ($\simeq$ 11.2%) have IRAS FSC counterparts. The difference is significant at $1.2 \times 10^{-13}$ ($\chi^2 = 62.8$) chance probability. The considerably lower detection rate of BLS1, however, may be due to the presence of faint Seyfert 1 galaxies. In order to overcome this effect, we constructed a control BLS1 sample with size 4 times as large as the NLS1 sample by one-to-one matching the optical $V$ magnitude and redshift of BLS1 to those of NLS1, as was done in the last section. For this subsample of 820 BLS1s, 181 sources have IRAS FSC counterparts, or $\approx$ 22.1%. The detection rate is larger than for the whole sample, but the difference between NLS1s and BLS1s is still significant at a 2% ($\chi^2 = 5.7$) chance probability. This suggests that NLS1s are brighter than BLS1s in the middle and far infrared bands.

For the objects detected by IRAS, we also compared the 60 $\mu$m and 100 $\mu$m luminosity distributions of BLS1 and NLS1s. The NLS1 appears more luminous in these wavelengths:

($\langle L_{60\mu\mathrm{m;\,NLS1}}\rangle = 24.67 \pm 0.09\,\mathrm{W\,Hz^{-1}}$, $\langle L_{60\mu\mathrm{m;\,BLS1}}\rangle = 24.49 \pm 0.05\,\mathrm{W\,Hz^{-1}}$, $\langle L_{100\mu\mathrm{m;\,NLS1}}\rangle = 25.02 \pm 0.12\,\mathrm{W\,Hz^{-1}}$ and $\langle L_{100\mu\mathrm{m;\,BLS1}}\rangle = 24.81 \pm 0.07\,\mathrm{W\,Hz^{-1}}$), consistent with their differing the detection rates. The K-S test gives $D = 0.218$ and $D = 0.331$, which are marginally significant at 2% and 1% chance probability, for the 60 $\mu$m and 100 $\mu$m luminosities, respectively. Besides, there is marginal evidence that the NLS1s have a cooler average IRAS color: $\langle \log(f_{60\mu\mathrm{m}}/f_{25\mu\mathrm{m}})\rangle_{\mathrm{NLS1}} = 0.453 \pm 0.035$ and $\langle \log(f_{60\mu\mathrm{m}}/f_{25\mu\mathrm{m}})\rangle_{\mathrm{BLS1}} = 0.386 \pm 0.027$, the difference is significant at 2% chance probability according to the K-S test (Figure 4).

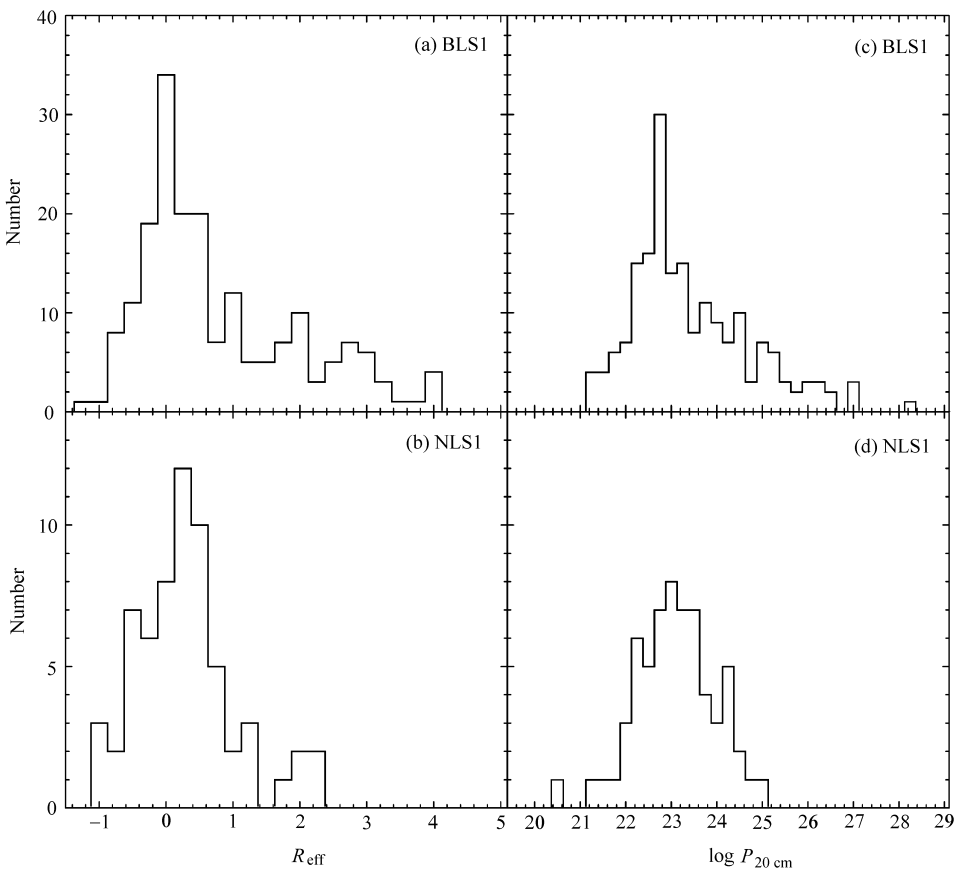


Fig. 3 Distribution of radio loudness for NLS1s (b & d) and control comparing sample of BLS1 (a & c). Note that the BLS1s show a bimodal distribution as in Fig. 1, while the NLS1s do not.

### 3.3 Near-IR Properties

We have seen in Section 2.2 that $109/205 \simeq 53.2\%$ NLS1s are detected by 2MASS, while $987/3236 \simeq 30.5\%$ BLS1s have 2MASS counterparts. For the control sample of 820 BLS1s used in Section 3.2, however, 411 BLS1s are detected by 2MASS ($\simeq 50.1\%$), similar to that of NLS1s and the 2MASS coverage rate. This means that, with the optical magnitudes of our NLS1 sample, most of the NLS1s and BLS1s can be detected in the Near-IR to the 2MASS limit.

It is found that NLS1s tend to show larger $J-K$ than BLS1s with similar $B-R$ (see Figure 5), which means that the K-excess is usually stronger in NLS1s than in BLS1s. However, the distributions of the other colors or luminosities are similar for NLS1s and BLS1s.

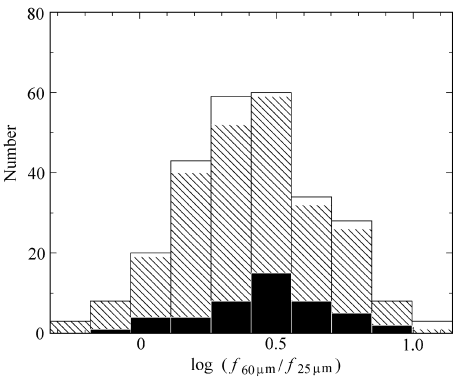


Fig. 4 Distribution of $f_{60\mu m}/f_{25\mu m}$ for NLS1s and control sample of BLS1.

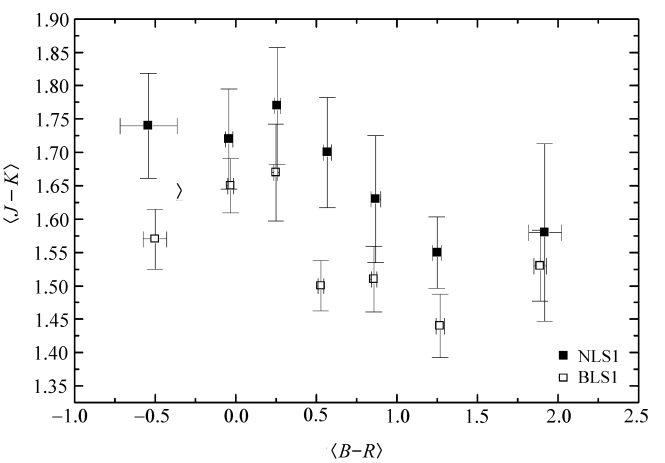


Fig. 5 $\langle J-K\rangle$ versus $\langle B-R\rangle$ diagram for NLS1s and the control sample of BLS1s. Clearly, NLS1s show systematically larger $J-K$ (K excess) than the BLS1s.

### 3.4 X-ray Spectrum

A correlation between the ROSAT photon index and the FWHM of the H$\beta$ line is now well established for Seyfert 1 galaxies and QSOs (Laor et al. 1994; Boller et al. 1996; Wang et al. 1996). Seyfert 1 galaxies with large H$\beta$ widths (FWHM H$\beta > 2000\,\mathrm{km\ s^{-1}}$) show a relatively small intrinsic scatter in their values of the photon index with a mean of $2.36 \pm 0.02$. NLS1s display a larger dispersion in their values of the photon index with a steep mean spectrum

$2.80 \pm 0.04$. Some of the NLS1s exhibit values of the photon index up to about 5, while about a fourth (45) display relative flat spectra with photon indexes of $\Gamma \leq 2.5$. We still do not know whether the flatness of X-ray in these NLS1s is intrinsic or is due to internal absorption. Apparently, some of the NLS1s are intrinsically absorbed (see Figure 6) and are listed in Table 4. A free $N_{\rm H}^{\rm F}$ fit to the 28 of 45 sources with relative flat ROSAT spectra ($\Gamma \leq 2.5$) yields ill-defined absorption column density due to the poor data quality; therefore, the fit is not meaningful. For the rest 17 objects, 12 have $\Gamma^{\rm F} > 2.5$, and five objects have $\Gamma^{\rm F} < 2.5$. Among the latter

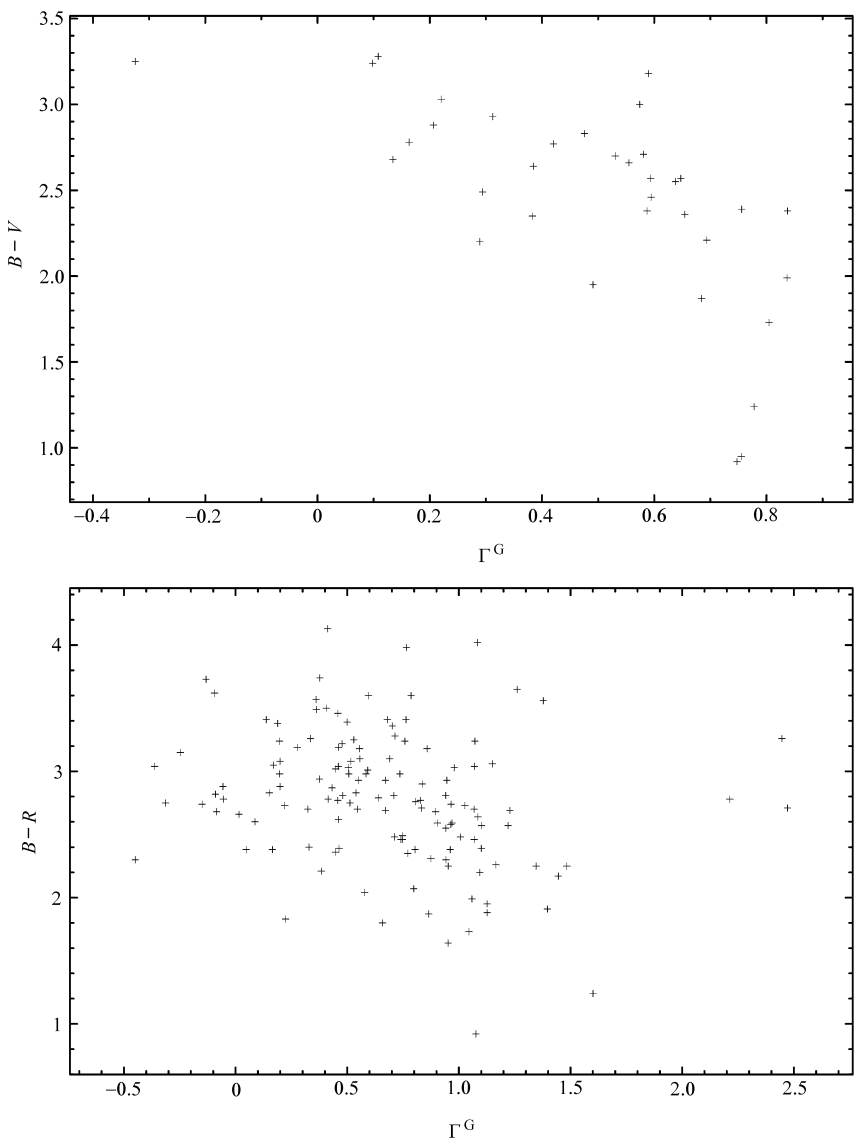


Fig. 6 Plots of $\Gamma$ versus $B-V$ and $B-R$. Objects with flat X-ray spectra show redder $B-V$ and $B-R$ colors.

five, the radio loud NLS1 2 E1640+5345 was classified as an ultra-soft source based on the Einstein data (Puchnarewicz et al. 1995) but with relative flat spectrum $\Gamma \simeq 2.0$ during the ROSAT observation. The situation may be similar to another radio loud NLS1, HE 0132–4313, which was found to show large spectral variations in the ROSAT band: it was very steep during the RASS but flat during the pointed observation (Grupe et al. 1999). Since the quality of spectrum is much higher in the pointed observation than in RASS, we adopted the former. However, The free $N_{\rm H}^{\rm F}$ fit to this object is not good. Large complex absorption was found in the ASCA spectrum of Mark 507 (Brandt et al. 1998), in which no significant intrinsic absorption was obtained in the free $N_{\rm H}$ fit to the ROSAT spectrum. NPM1G −14.0512 and ESO 399−IG20 have a large intrinsic/Galactic absorption column density, but the column density is not large enough to account for the flat spectrum. With the absorption column density of $\geq 7\times10^{20}{\rm cm}^{-2}$, however, the ROSAT can actually only detect the spectrum at energy $E > 0.8$ keV. On account of the X-ray spectrum of NLS1 being usually curved (soft X-ray excess, e.g., Leighly 1999), the

**Table 4** NLS1s with Significant Intrinsic Soft X-ray Absorption

| Common Name | $\Gamma^{\rm G}$ | $N_{\rm H}^{\rm G}$ | $\Gamma^{\rm free}$ | $N_{\rm H}^{\rm intrinsic}$ |
|---|---|---|---|---|
| | | $10^{20}\,{\rm cm}^{-2}$ | | $10^{20}\,{\rm cm}^{-2}$ |
| RXS J00323+2423 | $2.25^{+0.31}_{-0.33}$ | 3.39 | $4.40^{+>1.55}_{-2.21}$ | $7.27^{+>9.60}_{-7.20}$ |
| MARK 957 | $2.21^{+0.07}_{-0.04}$ | 6.18 | $3.28^{+0.26}_{-0.19}$ | $6.15^{+1.70}_{-1.60}$ |
| I Zw 1 | $2.49^{+0.04}_{-0.04}$ | 4.99 | $3.16^{+0.18}_{-0.17}$ | $2.54^{+0.70}_{-0.70}$ |
| | $2.58^{+0.11}_{-0.12}$ | | $3.83^{+0.76}_{-0.71}$ | $2.5^{+0.7}_{-0.7}$ |
| MARK 359 | $2.54^{+0.12}_{-0.12}$ | 4.8 | $3.24^{+0.63}_{-0.60}$ | $2.68^{+2.40}_{-2.10}$ |
| MARK 1239 | $2.7^{+0.07}_{-0.07}$ | 4.03 | $3.66^{+0.45}_{-0.43}$ | $3.18^{+1.50}_{-1.40}$ |
| KUG 1031+398 | $3.19^{+0.08}_{-0.07}$ | 1.02 | $4.17^{+0.74}_{-0.65}$ | $2.35^{+1.70}_{-1.50}$ |
| MARK 739E | $0.92^{+0.03}_{-0.03}$ | 1.89 | $2.64^{+0.12}_{-0.13}$ | $8.22^{+0.70}_{-0.80}$ |
| | $0.70^{+0.12}_{-0.15}$ | | $2.02^{+0.69}_{-0.67}$ | $5.2^{+3.6}_{-2.8}$ |
| | $0.76^{+0.06}_{-0.07}$ | | $2.01^{+0.28}_{-0.29}$ | $4.9^{+1.4}_{-1.2}$ |
| MCG 06.26.012 | $2.78^{+0.09}_{-0.09}$ | 2.01 | $3.91^{+0.92}_{-0.82}$ | $3.09^{+2.60}_{-2.20}$ |
| NGC 4051 | $2.56^{+0.02}_{-0.03}$ | 1.32 | $3.36^{+0.16}_{-0.16}$ | $2.34^{+0.40}_{-0.40}$ |
| IC 3599 | $3.03^{+0.03}_{-0.03}$ | 1.29 | $4.89^{+0.41}_{-0.37}$ | $4.65^{+1.10}_{-1.10}$ |
| CSO 961 | $2.87^{+0.11}_{-0.1}$ | 0.99 | $4.27^{+1.18}_{-0.98}$ | $3.33^{+3.10}_{-2.30}$ |
| IRAS 13224−3809 | $3^{+0.03}_{-0.02}$ | 4.79 | $4.86^{+0.20}_{-0.21}$ | $5.83^{+0.70}_{-0.60}$ |
| RXS J14025+2159 | $2.69^{+0.14}_{-0.13}$ | 2.06 | $3.97^{+1.35}_{-1.15}$ | $3.74^{+3.90}_{-3.10}$ |
| PG 1404+226 | $3.08^{+0.05}_{-0.04}$ | 2.14 | $4.43^{+0.38}_{-0.36}$ | $3.84^{+1.10}_{-1.00}$ |
| RXS J15475+1024 | $3.1^{+0.17}_{-0.17}$ | 3.51 | $4.64^{+>1.34}_{-1.33}$ | $4.69^{+>4.50}_{-3.90}$ |
| B3 1702+457 | $1.94^{+0.06}_{-0.07}$ | 2.22 | $2.83^{+0.42}_{-0.41}$ | $2.73^{+1.40}_{-1.30}$ |
| RXS J20394-3018 | $2.28^{+0.15}_{-0.18}$ | 5.18 | $3.37^{+1.01}_{-0.87}$ | $4.54^{+3.90}_{-3.50}$ |
| RXS J21441-3949 | $3.18^{+0.16}_{-0.15}$ | 2.26 | $4.43^{+>1.56}_{-1.27}$ | $3.72^{+>4.30}_{-3.30}$ |
| II Zw 177 | $3.6^{+0.21}_{-0.2}$ | 5.41 | $5.42^{+>0.49}_{-1.47}$ | $6.00^{+>2.40}_{-4.60}$ |
| KAZ 320 | $1.64^{+0.12}_{-0.12}$ | 5.21 | $3.03^{+0.68}_{-0.60}$ | $6.52^{+4.80}_{-3.00}$ |
| MS 23409-1511 | $3.09^{+0.15}_{-0.14}$ | 2.2 | $5.09^{+>0.84}_{-1.22}$ | $5.43^{+>2.70}_{-3.20}$ |

flat spectrum observed by the ROSAT does not imply an intrinsic flat spectrum in the whole ROSAT band for these strongly absorbed sources. Therefore, it is very likely that most, if not all, of these sources are steep spectral sources. A statistical study yields marginally significant anti-correlation between $\Gamma$ and $N_{\rm H}^{\rm intrinsic} \equiv N_{\rm H}^{\rm F} - N_{\rm H}^{\rm G}$ ($r_s = -0.277$, $N = 62$, $P_r = 2.9\%$). However, the correlation is mostly due to the two flattest objects. When these two objects were not considered, there was no longer any correlation. Given the large uncertainties in the $N_{\rm H}^{\rm F}$ for most objects, this result is expected.

Since either warm or cold absorption gas may be mixed with dust, it may be advisable to compare the soft X-ray continuum spectrum with the optical color. The dependence on the optical colors are illustrated in Figure 6. NLS1s with flat soft X-ray spectrum tend to have redder $B - R$ colors. The Spearman correlation coefficient is $-0.424$ and correlation is significant at $3 \times 10^{-5}$ level for 89 objects with $\Gamma$ negative error less than 0.5. Though the number of objects with $B - V$ and $U - B$ in the VV01 is somewhat smaller, the $B - V$ and $U - B$ are usually obtained with a smaller aperture and are more accurate than the $B$ or $R$ magnitude in the USNO-A2 catalog. Apparently, $\Gamma$ is correlated with $B - V$ and $U - B$ with Spearman rank correlation coefficients $R_s = -0.708$ and –0.498 for 35 and 32 objects, which are significant at $2 \times 10^{-6}$ and 0.4%, respectively.

Therefore, our analysis suggests that the flatness of soft X-ray spectra of some NLS1s is due to intrinsic absorption and spectral variability, and that the actual scatter of the correlation between H$\beta$ line width and soft X-ray photon index is smaller than it appears. This may explain the different degrees of tightness of the correlation found for the BQS subsample, QSOs, and Seyfert galaxies (Laor et al. 1997; Wang et al. 1996; Boller et al. 1996) as the QSOs in the BQS sample are less absorbed.

### 3.5 Correlations of Broad Band Data

With these large datasets, we made correlation analyses among the luminosities, between the color and luminosity, as well as in color-color pairs, to find the relations between the continua in different bands and to compare the behaviors of the NLS1s, and the RL and RQ BLS1s. The advantage of this sample is its large size, so any weak correlation can hopefully be identified; its disadvantage is that it is an inhomogeneous sample, and may suffer from selection effects.

#### *3.5.1 Luminosity and luminosity correlations*

To eliminate spurious correlations due to the redshift effect, we calculate the partial correlation coefficient at fixed redshift:

$$r_{xy,z} = \frac{r_{xy} - (r_{xz})(r_{yz})}{\sqrt{(1 - r_{xz}^2)} \times \sqrt{(1 - r_{yz}^2)}}, \tag{1}$$

where $x$ and $y$ are the luminosities at the two bands considered, $z$ is the redshift, and $r_{xy}$, $r_{xz}$ and $r_{yz}$ are the correlation coefficients between $x$ and $y$, between $x$ and $z$, and between $y$ and $z$, respectively. In this subsection, all correlations are partial correlations. A summary of inter-band correlations is given in Table 5.

The optical and near-infrared luminosities are well correlated. The partial correlation coefficients are all larger than 0.5, the tightest one being $r = 0.839$ between $V$ and $J$ for NLS1. However, the far-infrared luminosities are very weak or are not correlated with the optical and X-ray luminosities (see Table 5). This indicates that far-infrared emission is dominated by emission from host galaxies.

**Table 5** Luminosity-Luminosity Correlation Matrix

| | $P_{6\rm cm}$ | $P_{20\rm cm}$ | $L_{12\mu\rm m}$ | $L_{25\mu\rm m}$ | $L_{60\mu\rm m}$ | $L_{100\mu\rm m}$ | $L_{K_s}$ | $L_{\rm H}$ | $L_J$ | $L_V$ | $L_{F_m}$ | $L_{B_J}$ | $L_X$ |
|---|---|---|---|---|---|---|---|---|---|---|---|---|---|
| NLS1s | | | | | | | | | | | | | |
| $L_{6\,\rm cm}$ | | 0.908 | 0.355 | 0.343 | 0.161 | 0.009 | 0.000 | 0.074 | 0.070 | 0.020 | –0.076 | –0.154 | –0.186 |
| $L_{20\,\rm cm}$ | 0.908 | | 0.550 | 0.562 | 0.388 | 0.296 | 0.322 | 0.422 | 0.419 | 0.270 | 0.247 | 0.213 | 0.063 |
| $L_{12\mu\rm m}$ | 0.355 | 0.550 | | 0.864 | 0.512 | 0.372 | 0.592 | 0.556 | 0.651 | 0.396 | 0.063 | 0.110 | 0.221 |
| $L_{25\mu\rm m}$ | 0.343 | 0.562 | 0.864 | | 0.608 | 0.371 | 0.629 | 0.571 | 0.571 | 0.345 | 0.154 | 0.091 | 0.205 |
| $L_{60\mu\rm m}$ | 0.161 | 0.388 | 0.512 | 0.608 | | 0.857 | 0.379 | 0.426 | 0.434 | 0.264 | 0.284 | 0.247 | –0.172 |
| $L_{100\mu\rm m}$ | 0.009 | 0.296 | 0.372 | 0.371 | 0.857 | | 0.452 | 0.468 | 0.386 | 0.023 | 0.172 | 0.070 | –0.250 |
| $L_{K_s}$ | 0.000 | 0.322 | 0.592 | 0.629 | 0.379 | 0.452 | | 0.974 | 0.940 | 0.808 | 0.568 | 0.617 | 0.470 |
| $L_{\rm H}$ | 0.074 | 0.422 | 0.556 | 0.571 | 0.426 | 0.468 | 0.974 | | 0.969 | 0.830 | 0.584 | 0.620 | 0.428 |
| $L_J$ | 0.070 | 0.419 | 0.651 | 0.571 | 0.434 | 0.386 | 0.940 | 0.969 | | 0.839 | 0.633 | 0.671 | 0.470 |
| $L_V$ | 0.020 | 0.270 | 0.396 | 0.345 | 0.264 | 0.023 | 0.808 | 0.830 | 0.839 | | 0.546 | 0.608 | 0.493 |
| $L_{F_m}$ | –0.076 | 0.247 | 0.063 | 0.154 | 0.284 | 0.172 | 0.568 | 0.584 | 0.633 | 0.546 | | 0.920 | 0.299 |
| $L_{B_J}$ | –0.154 | 0.213 | 0.110 | 0.091 | 0.247 | 0.070 | 0.617 | 0.620 | 0.671 | 0.608 | 0.920 | | 0.350 |
| $L_X$ | –0.186 | 0.063 | 0.221 | 0.205 | –0.172 | –0.250 | 0.470 | 0.428 | 0.470 | 0.493 | 0.299 | 0.350 | |
| RQ BLS1s | | | | | | | | | | | | | |
| $\rm P_{6\mathit{cm}}$ | | 0.794 | 0.355 | 0.222 | 0.262 | 0.499 | 0.051 | 0.132 | 0.108 | 0.111 | 0.193 | 0.199 | –0.130 |
| $\rm P_{20\mathit{cm}}$ | 0.794 | | 0.602 | 0.650 | 0.578 | 0.702 | 0.352 | 0.362 | 0.371 | 0.427 | 0.312 | 0.343 | 0.234 |
| $L_{12\mu\rm m}$ | 0.355 | 0.602 | | 0.828 | 0.375 | 0.411 | 0.741 | 0.702 | 0.678 | 0.344 | 0.045 | 0.144 | 0.336 |
| $L_{25\mu\rm m}$ | 0.222 | 0.650 | 0.828 | | 0.625 | 0.534 | 0.588 | 0.552 | 0.548 | 0.440 | 0.185 | 0.270 | 0.338 |
| $L_{60\mu\rm m}$ | 0.262 | 0.578 | 0.375 | 0.625 | | 0.885 | 0.241 | 0.229 | 0.170 | 0.190 | 0.140 | 0.178 | 0.071 |
| $L_{100\mu\rm m}$ | 0.499 | 0.702 | 0.411 | 0.534 | 0.885 | | 0.388 | 0.368 | 0.320 | 0.229 | 0.131 | 0.163 | 0.184 |
| $L_{K_s}$ | 0.051 | 0.352 | 0.741 | 0.588 | 0.241 | 0.388 | | 0.969 | 0.941 | 0.678 | 0.576 | 0.581 | 0.516 |
| $L_{\rm H}$ | 0.132 | 0.362 | 0.702 | 0.552 | 0.229 | 0.368 | 0.969 | | 0.968 | 0.677 | 0.614 | 0.609 | 0.470 |
| $L_J$ | 0.108 | 0.371 | 0.678 | 0.548 | 0.170 | 0.320 | 0.941 | 0.968 | | 0.697 | 0.617 | 0.608 | 0.474 |
| $L_V$ | 0.111 | –0.427 | 0.344 | 0.440 | 0.190 | 0.229 | 0.678 | 0.677 | 0.697 | | 0.580 | 0.602 | 0.545 |
| $L_{F_m}$ | 0.193 | 0.312 | 0.045 | 0.185 | 0.140 | 0.131 | 0.576 | 0.614 | 0.617 | 0.580 | | 0.923 | 0.298 |
| $L_{B_J}$ | 0.199 | 0.343 | 0.144 | 0.270 | 0.178 | 0.163 | 0.581 | 0.609 | 0.608 | 0.602 | 0.923 | | 0.352 |
| $L_X$ | –0.130 | 0.234 | 0.336 | 0.338 | 0.071 | 0.184 | 0.516 | 0.470 | 0.474 | 0.545 | 0.298 | 0.352 | |
| RL BLS1s | | | | | | | | | | | | | |
| $\rm P_{6\mathit{cm}}$ | | 0.874 | –0.197 | –0.112 | –0.303 | –0.022 | 0.272 | 0.263 | 0.286 | 0.232 | 0.244 | 0.323 | 0.551 |
| $\rm P_{20\mathit{cm}}$ | 0.874 | | –0.146 | –0.014 | –0.086 | –0.009 | 0.326 | 0.338 | 0.376 | 0.397 | 0.339 | 0.375 | 0.443 |
| $L_{12\mu\rm m}$ | –0.197 | –0.146 | | 0.881 | 0.808 | | 0.264 | 0.584 | 0.584 | 0.185 | 0.576 | 0.518 | –0.195 |
| $L_{25\mu\rm m}$ | –0.112 | –0.014 | 0.881 | | 0.868 | 0.752 | 0.264 | 0.323 | 0.324 | 0.316 | 0.642 | 0.668 | –0.343 |
| $L_{60\mu\rm m}$ | –0.303 | –0.086 | 0.808 | 0.868 | | 0.859 | 0.209 | 0.343 | 0.279 | 0.205 | 0.550 | 0.617 | –0.117 |
| $L_{100\mu\rm m}$ | –0.022 | –0.009 | | 0.752 | 0.859 | | 0.822 | 0.822 | 0.756 | 0.402 | 0.621 | 0.757 | 0.000 |
| $L_{K_s}$ | 0.272 | 0.326 | 0.584 | 0.264 | 0.209 | 0.822 | | 0.960 | 0.904 | 0.705 | 0.650 | 0.728 | 0.558 |
| $L_{\rm H}$ | 0.263 | 0.338 | 0.584 | 0.323 | 0.343 | 0.822 | 0.960 | | 0.961 | 0.697 | 0.691 | 0.753 | 0.547 |
| $L_J$ | 0.286 | 0.376 | 0.584 | 0.324 | 0.279 | 0.756 | 0.904 | 0.961 | | 0.713 | 0.715 | 0.772 | 0.557 |
| $L_V$ | 0.232 | 0.397 | 0.185 | 0.316 | 0.205 | 0.402 | 0.705 | 0.697 | 0.713 | | 0.637 | 0.682 | 0.603 |
| $L_{F_m}$ | 0.244 | 0.339 | 0.576 | 0.642 | 0.550 | 0.621 | 0.650 | 0.691 | 0.715 | 0.637 | | 0.907 | 0.510 |
| $L_{B_J}$ | 0.323 | 0.375 | 0.518 | 0.668 | 0.617 | 0.757 | 0.728 | 0.753 | 0.772 | 0.682 | 0.907 | | 0.541 |
| $L_X$ | 0.551 | 0.443 | –0.195 | –0.343 | –0.117 | 0.000 | 0.558 | 0.547 | 0.557 | 0.603 | 0.510 | 0.541 | |

The NIR luminosities are well-correlated with the mid-infrared luminosities from IRAS, but are only marginally so with the far-infrared luminosities. No significant difference is found among the RL and RQ BLS1s and NLS1s on these correlations. For RQ BLS1s, the far-infrared luminosity is well correlated with the radio luminosity, but this correlation is absent for RL BLS1s. The radio power at 20 cm and the X-ray luminosities are significant correlated for the RL objects ($R_{rx,z} = 0.443$, $n = 151$, $P = 10^{-8}$), while only a weak correlation is found for RQ objects ($R_{rx,z} = 0.234$, $n = 272$, $P = 10^{-4}$) and it is absent for NLS1s ($R_{rx,z} = 0.063$, $n = 61$,

$P = 0.6$). This might indicate that the 20 cm radio emission is dominated by an extended component in RQ BLS1s.

The optical, near-infrared luminosities are all correlated with the X-ray luminosity. Among the various luminosities, the $V$ magnitude from VV01 correlates best with the X-ray flux, next with the near-infrared fluxes. The optical magnitude from GSC2.2 are less well correlated with the X-ray flux, especially for RQ BLS1s. The partial correlation coefficient ranges from only 0.227 to 0.352 from $F$ to $B_J$, compared with $r = 0.545$ with $V$ magnitude from VV01. This is most likely due to the inclusion of extended emission from the galaxies. A plot does show that the optical magnitude from GSC2.2 is much larger than those in VV01 for a significant number of objects, particularly for the RQ BLS1s (Figure 7). The difference is smaller for RL objects and the NLS1s.

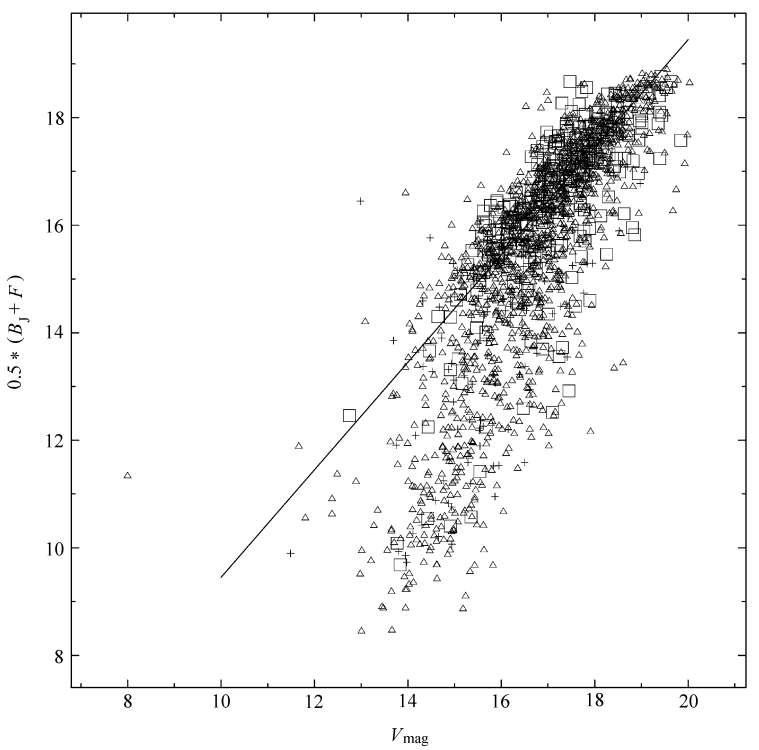


Fig. 7 Plot of $V$ magnitudes from VV01 versus $V_{\rm GSC} \simeq \frac{1}{2}(F + B_J)$ from GSC 2.2 (Legends: crosses–NLS1; triangles–RQ BLS1; squares–RL BLS1s). The solid line is the line $V_{\rm mag} = V_{\rm GSC} + 0.55$ drawn to guide the eye. It is clear that for bright objects, the $V_{\rm GSC}$ depart systematically from the linear relation, due to contamination of the star light.

### *3.5.2 Luminosity-color correlation*

In this subsection, the colors are defined as flux ratios between two bands. Since our previous analysis shows that the magnitude from GSC2.2 is more likely contaminated by star light in the host galaxies, so we use the optical colors $U-B$ and $B-V$ from VV01. The mid-to-far infrared color is the ratio of $R_{60-25}$=log($f_{60\mu{\rm m}}/f_{25\mu{\rm m}}$. Other quantities are radio spectral

index $f_{20\,\mathrm{cm}}/f_{6\,\mathrm{cm}}$, $R_{\mathrm{eff}}$, $R_{X-V}$=log($f_X/f_V$), and $R_{60-K}$ = log($f_{60\mu\mathrm{m}}/f_{K_s}$). The correlation coefficients are summarized in Table 6.

**Table 6** Luminosity-Color Correlation Matrix

| | $\alpha_{6-20\,\mathrm{cm}}$ | $R_{60-25}$ | $J-K_s$ | $H-K_s$ | $J-H$ | $B-V$ | $U-B$ | $B-K_s$ | $R_{60-K_s}$ | $R_{\mathrm{eff}}$ | $R_{X-V}$ | $\Gamma^{\mathrm{G}}$ |
|---|---|---|---|---|---|---|---|---|---|---|---|---|
| NLS1s | | | | | | | | | | | | |
| $L_{6\,\mathrm{cm}}$ | −0.396 | −0.288 | −0.482 | −0.473 | −0.400 | −0.370 | −0.345 | 0.433 | 0.214 | 0.787 | 0.331 | 0.080 |
| $L_{20\,cm}$ | −0.291 | −0.230 | 0.204 | 0.211 | 0.102 | −0.092 | 0.005 | 0.499 | 0.363 | 0.753 | 0.281 | 0.052 |
| $L_{12\,\mu\mathrm{m}}$ | −0.059 | −0.632 | 0.501 | 0.538 | 0.387 | −0.489 | −0.346 | 0.800 | 0.193 | 0.335 | 0.289 | 0.195 |
| $L_{25\mu\mathrm{m}}$ | −0.103 | −0.245 | 0.544 | 0.623 | 0.268 | −0.579 | −0.367 | 0.650 | 0.160 | 0.422 | 0.225 | 0.118 |
| $L_{60\mu\mathrm{m}}$ | −0.028 | 0.143 | 0.372 | 0.398 | 0.217 | −0.312 | −0.125 | 0.539 | 0.481 | 0.475 | 0.205 | 0.078 |
| $L_{100\mu\mathrm{m}}$ | −0.096 | 0.280 | 0.460 | 0.483 | 0.360 | −0.118 | 0.174 | 0.768 | 0.685 | 0.559 | 0.130 | 0.006 |
| $L_{K_s}$ | −0.286 | −0.374 | 0.677 | 0.744 | 0.306 | −0.418 | −0.321 | 0.555 | −0.099 | 0.029 | 0.140 | 0.155 |
| $L_{\mathrm{H}}$ | −0.334 | −0.342 | 0.603 | 0.658 | 0.279 | −0.377 | −0.344 | 0.555 | −0.034 | 0.082 | 0.120 | 0.119 |
| $L_J$ | −0.407 | −0.321 | 0.520 | 0.627 | 0.155 | −0.424 | −0.379 | 0.510 | 0.007 | 0.067 | 0.138 | 0.127 |
| $L_V$ | 0.157 | −0.237 | 0.519 | 0.611 | 0.161 | −0.461 | −0.409 | 0.367 | −0.016 | 0.046 | 0.014 | 0.220 |
| $L_{F_m}$ | 0.361 | 0.106 | 0.200 | 0.275 | −0.041 | 0.074 | 0.160 | −0.406 | −0.177 | −0.272 | −0.190 | −0.001 |
| $L_{B_J}$ | 0.495 | 0.068 | 0.274 | 0.386 | −0.037 | 0.015 | 0.053 | −0.361 | −0.176 | −0.287 | −0.170 | 0.026 |
| $L_X$ | −0.004 | −0.367 | 0.529 | 0.620 | 0.145 | −0.738 | −0.681 | 0.544 | −0.085 | 0.325 | 0.603 | 0.581 |
| RQ BLS1s | | | | | | | | | | | | |
| $L_{6\,\mathrm{cm}}$ | −0.442 | −0.212 | −0.088 | 0.101 | −0.226 | −0.527 | −0.328 | 0.467 | 0.018 | 0.548 | 0.209 | −0.170 |
| $L_{11\,\mathrm{cm}}$ | −0.479 | −0.600 | −0.583 | −0.285 | −0.627 | −0.517 | −0.304 | 0.199 | −0.262 | 0.559 | 0.311 | −0.141 |
| $L_{20\,\mathrm{cm}}$ | −0.160 | −0.182 | 0.360 | 0.452 | 0.051 | −0.476 | −0.492 | 0.650 | 0.191 | 0.640 | 0.195 | −0.128 |
| $L_{12\mu\mathrm{m}}$ | 0.043 | −0.406 | 0.594 | 0.656 | 0.248 | −0.456 | −0.483 | 0.745 | −0.205 | 0.326 | 0.235 | −0.092 |
| $L_{25\mu\mathrm{m}}$ | −0.047 | −0.345 | 0.408 | 0.542 | 0.039 | −0.516 | −0.555 | 0.719 | −0.044 | 0.386 | 0.291 | 0.003 |
| $L_{60\mu\mathrm{m}}$ | 0.026 | 0.047 | 0.471 | 0.516 | 0.222 | −0.417 | −0.421 | 0.719 | 0.401 | 0.451 | 0.240 | −0.062 |
| $L_{100\mu\mathrm{m}}$ | −0.065 | 0.114 | 0.389 | 0.395 | 0.153 | −0.433 | −0.457 | 0.712 | 0.506 | 0.521 | 0.237 | 0.071 |
| $L_{K_s}$ | −0.033 | −0.499 | 0.547 | 0.610 | 0.182 | −0.646 | −0.565 | 0.561 | −0.159 | 0.328 | 0.136 | −0.004 |
| $L_{\mathrm{H}}$ | −0.066 | −0.470 | 0.472 | 0.513 | 0.179 | −0.627 | −0.562 | 0.542 | −0.135 | 0.328 | 0.117 | −0.017 |
| $L_J$ | −0.054 | −0.462 | 0.408 | 0.511 | 0.070 | −0.629 | −0.559 | 0.534 | −0.138 | 0.333 | 0.125 | −0.014 |
| $L_V$ | −0.135 | −0.334 | 0.378 | 0.473 | 0.048 | −0.658 | −0.121 | 0.370 | −0.007 | 0.053 | −0.113 | 0.073 |
| $L_{F_m}$ | 0.189 | 0.082 | 0.067 | 0.040 | 0.081 | 0.074 | 0.166 | −0.429 | −0.197 | −0.367 | −0.272 | 0.064 |
| $L_{B_J}$ | 0.277 | 0.075 | 0.075 | 0.061 | 0.062 | −0.019 | 0.122 | −0.491 | −0.195 | −0.343 | −0.239 | 0.111 |
| $L_X$ | 0.007 | −0.421 | 0.447 | 0.580 | 0.037 | −0.728 | −0.686 | 0.501 | −0.052 | 0.193 | 0.502 | 0.437 |
| RL BLS1s | | | | | | | | | | | | |
| $L_{6\,\mathrm{cm}}$ | 0.174 | −0.250 | −0.271 | −0.081 | −0.390 | −0.107 | 0.053 | 0.030 | −0.212 | 0.702 | −0.084 | −0.046 |
| $L_{11\,\mathrm{cm}}$ | 0.323 | 0.273 | −0.338 | −0.228 | −0.367 | −0.108 | 0.073 | 0.139 | 0.000 | 0.616 | −0.030 | −0.140 |
| $L_{20\,\mathrm{cm}}$ | 0.438 | −0.204 | −0.298 | −0.131 | −0.365 | −0.183 | −0.031 | −0.027 | 0.020 | 0.824 | −0.192 | −0.002 |
| $L_{12\mu\mathrm{m}}$ | 0.011 | 0.345 | −0.086 | −0.086 | −0.314 | −0.286 | −0.048 | 0.100 | 0.000 | −0.020 | −0.119 | 0.059 |
| $L_{25\mu\mathrm{m}}$ | 0.229 | 0.507 | 0.000 | 0.117 | −0.083 | −0.550 | −0.079 | 0.300 | 0.467 | 0.033 | 0.218 | 0.134 |
| $L_{60\mu\mathrm{m}}$ | 0.154 | 0.726 | 0.077 | 0.037 | 0.090 | −0.612 | −0.212 | 0.091 | 0.503 | −0.131 | 0.308 | −0.198 |
| $L_{100\mu\mathrm{m}}$ | 0.133 | 0.427 | 0.738 | 0.810 | 0.595 | 0.000 | 0.200 | 0.800 | −0.167 | −0.261 | −0.300 | −0.049 |
| $L_{K_s}$ | 0.100 | −0.300 | −0.150 | 0.027 | −0.284 | −0.284 | −0.097 | −0.001 | −0.411 | 0.360 | −0.293 | 0.153 |
| $L_{\mathrm{H}}$ | 0.112 | −0.183 | −0.246 | −0.095 | −0.319 | −0.281 | −0.103 | −0.029 | −0.332 | 0.381 | −0.297 | 0.137 |
| $L_J$ | 0.126 | −0.067 | −0.329 | −0.126 | −0.422 | −0.290 | −0.085 | −0.056 | −0.288 | 0.399 | −0.268 | 0.154 |
| $L_V$ | 0.097 | −0.147 | −0.280 | −0.063 | −0.410 | −0.253 | −0.105 | −0.125 | 0.055 | 0.151 | −0.438 | 0.174 |
| $L_{F_m}$ | 0.124 | 0.121 | −0.353 | −0.144 | −0.366 | 0.060 | 0.118 | −0.475 | −0.127 | 0.214 | −0.344 | 0.126 |
| $L_{B_J}$ | 0.159 | 0.300 | −0.306 | −0.089 | −0.377 | −0.026 | −0.005 | −0.511 | 0.042 | 0.258 | −0.385 | 0.114 |
| $L_X$ | 0.189 | 0.370 | −0.255 | −0.010 | −0.423 | −0.257 | −0.097 | −0.055 | −0.257 | 0.368 | 0.046 | 0.246 |

For NLS1s and RQ BLS1s, the optical colors ($U-B$ and $B-V$) are anti-correlated with NIR, optical, X-ray and radio luminosities, and the colors $H-K$ and $V-K$ are positively correlated with these luminosities. In other words, the luminous objects show blue optical colors and red $H-K$ colors (Figure 8). However, there are no such correlations for RL BLS1s.

Instead, there is a weak anti-correlation between the $J - H$ and the X-ray, NIR, optical and radio luminosities, which is absent in RQ NLS1s.

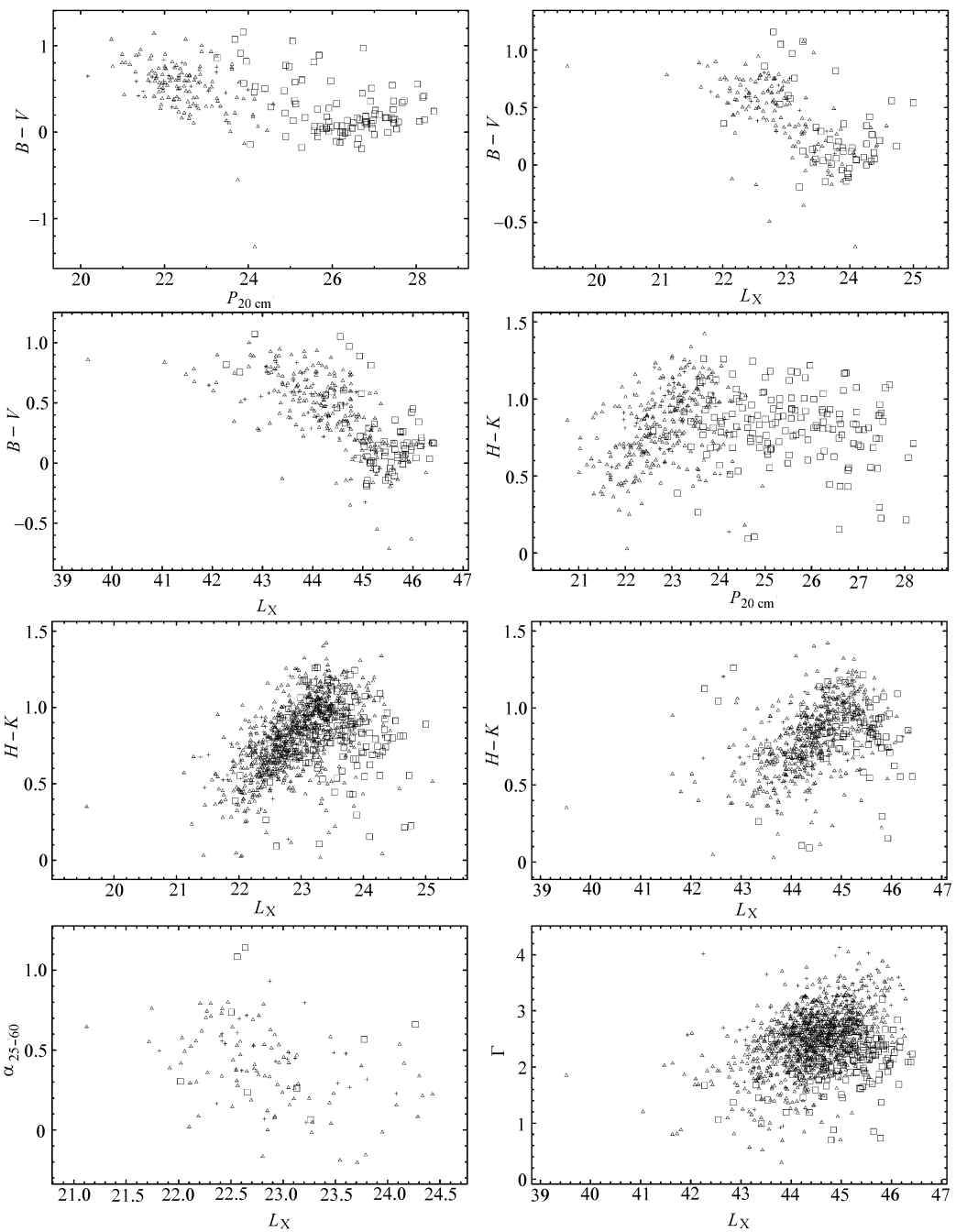


Fig. 8 Luminosity-color diagrams for NLS1s (crosses), RL BLS1s (squares) and RQ BLS1s (triangles).

No significant correlation was found between the radio spectral index and any of the luminosities for the NLS1s, RQ and RL BLS1s. There is a significant anti-correlation between $\alpha_{25-60}$ and the optical, NIR and X-ray luminosities for radio quiet objects, i.e., more luminous objects tend to have warmer IRAS colors. This is not a new relation (Bonatto & Pastoriza 1997). There is a similar size correlation for the NLS1s, but the small number of objects makes this correlation non-significant.

In the ROSAT band ($0.2-2.4\,\mathrm{keV}$), the X-ray luminosity is well correlated with the spectral index for the NLS1 galaxies ($R_s = 0.581$, $P_s = 10^{-15}$) and RQ BLS1s ($R_s = 0.437$, $P_s < 10^{-20}$), but such a correlation is barely significant for the RL objects ($R_s = 0.246$, $P_s = 0.2\%$).

### *3.5.3 Color-Color correlations*

The color-color correlation coefficients are listed in Table 7. The NLS1s and RQ BLS1s show similar color-color correlations, but the RL BLS1s are a little different. The optical colors $U-B$ and $B-V$ are anti-correlated with the X-ray photon index $\Gamma$ and with $R_{X-V}$ for the NLS1s and RQ BLS1s (Figure 9). This was interpreted in the last section as evidence for the role of absorption and reddening in NLS1s, and the presence of these anti-correlations in the RQ BLS1s suggests that absorption and reddening are also important in the latter. The RL BLS1s also show an anti-correlation between $(U-B)/(B-V)$ and $\Gamma$, but no correlation between $(U-B)/(B-V)$ and $R_{X-V}$. $H-K$, but not $J-H$, is anti-correlated with $B-V$ for the NLS1s and RQ BLS1s. This can be due either to contamination of stellar light from the bulge of host galaxies in the $H$ and $V$ bands since the bulge stars contribute more at the $V$ and $H$ bands than at the $B$ and $K$ bands, or to reddening and associated dust emission at K band. $\Gamma$ is also weakly correlated with H-K and $f_{X-V}$ for the NLS1s, and RQ and RL BLS1s. We did not find any significant correlation between the radio spectral index and any other colors. For the NLS1s and RQ BLS1s, the infrared color $R_{25-60}$ is correlated with $B-V$ and anti-correlated with $H-K$ and $B-K$. If $R_{25-60}$ is an indicator of the relative contribution of AGN to the emission of the galaxy, then this correlation implies that weak AGNs have red $B-V$ and blue $H-K$. That no such correlation was found for the RL BLS1s may be due to their small sample size. $B-K$ is moderately strongly correlated with $H-K$ and $J-K$ for the NLS1s, and RQ and RL BLS1s. In addition, $R_{X-V}$ is correlated with $\Gamma$ for the NLS1s, and RQ and RL BLS1s (strongest for the first). This correlation is likely to be an artefact. Since the X-ray flux is calculated from the fitted $\Gamma$, overestimation of $\Gamma$ may lead to an over-large X-ray flux, hence an over-large $R_{X-V}$; and vice verse.

Radio loud quasars also have stronger X-ray emission than radio quiet quasars (e.g., Brinkmann et al. 1997). It was found that the radio loudness of NLS1s and RQ BLS1s is correlated with $R_{X-V}$. The Spearman correlation coefficient is 0.359 for the NLS1s and 0.345 for the RQ BLS1s, respectively, at chance probabilities 0.6% and $10^{-8}$. However, the RL BLS1s do not show such a correlation. This suggests that the stronger X-ray emission in RL objects is a consequence of continuous increasing of the ratio $R_{X-V}$ with the radio loudness for radio quiet objects.

Radio-loud quasars are well known to have flatter X-ray spectral indexes than radio-quiet ones (e.g. Yuan, Brinkmann & Siebert 1998; Lawson & Turner, 1997). However, we did not find such relation for NLS1s. Radio loudness $R_{\mathrm{eff}}$ is only weakly anti-correlated with photon index $\Gamma$ for BLS1s. The Spearman correlation coefficient is $-0.222$ for BLS1s, with a chance probability of $10^{-6}$ ($n = 483$). While for the 64 NLS1s observed in X-ray (ROSAT)and radio (47 sources by NVSS and 17 by FIRST), such a relation is not significant. However, this only

reflects the fact that radio loud objects have flat X-ray spectrum than radio quite ones, and the correlation does not exist within RL BLS1s or RQ BLS1s, separately.

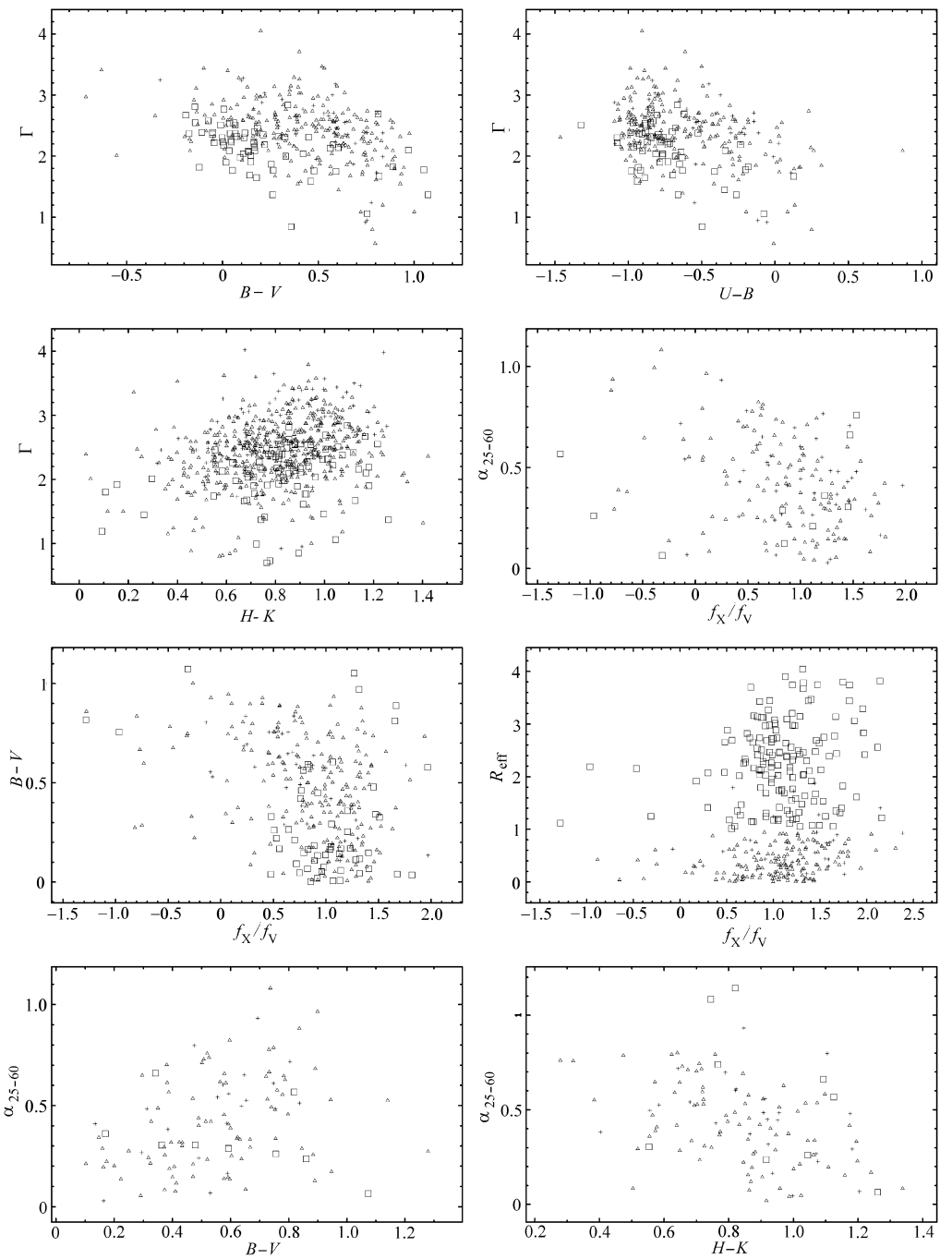


Fig. 9 Color-color diagrams for NLS1s and BLS1s (Legends are as for Figure 8).

**Table 7** Color-Color Correlation Matrix

| | $\alpha_{6-20\,\mathrm{cm}}$ | $R_{60-25}$ | $J-K_s$ | $H-K_s$ | $J-H$ | $B-V$ | $U-B$ | $B-K_s$ | $R_{60-K_s}$ | $R_{\mathrm{eff}}$ | $R_{X-V}$ | $\Gamma^{\mathrm{G}}$ |
|---|---|---|---|---|---|---|---|---|---|---|---|---|
| NLS1s | | | | | | | | | | | | |
| $\alpha_{6-20\,\mathrm{cm}}$ | | −0.251 | 0.541 | 0.213 | 0.590 | −0.228 | | 0.107 | 0.180 | −0.433 | −0.122 | −0.256 |
| $R_{60-25}$ | −0.251 | | −0.431 | −0.492 | −0.331 | 0.565 | −1.000 | −0.465 | 0.585 | 0.069 | −0.292 | 0.008 |
| $J-K_s$ | 0.541 | −0.431 | | 0.875 | 0.749 | −0.405 | −1.000 | 0.515 | −0.270 | −0.242 | 0.163 | 0.225 |
| $H-K_s$ | 0.213 | −0.492 | 0.875 | | 0.391 | −0.567 | −1.000 | 0.408 | −0.304 | −0.294 | 0.203 | 0.386 |
| $J-H$ | 0.590 | −0.331 | 0.749 | 0.391 | | −0.167 | 1.000 | 0.472 | −0.186 | −0.133 | 0.015 | −0.052 |
| $B-V$ | −0.228 | 0.565 | −0.405 | −0.567 | −0.167 | | 1.000 | −0.370 | 0.332 | −0.321 | −0.727 | −0.708 |
| $U-B$ | | −1.000 | −1.000 | −1.000 | 1.000 | 1.000 | | −0.381 | 0.455 | −0.400 | −0.653 | −0.498 |
| $B-K_s$ | 0.107 | −0.465 | 0.515 | 0.408 | 0.472 | −0.370 | −0.381 | | −0.019 | −0.011 | 0.335 | 0.309 |
| $R_{60-K_s}$ | 0.180 | 0.585 | −0.270 | −0.304 | −0.186 | 0.332 | 0.455 | −0.019 | | 0.244 | −0.221 | −0.127 |
| $R_{\mathrm{eff}}$ | −0.433 | 0.069 | −0.242 | −0.294 | −0.133 | −0.321 | −0.400 | −0.011 | 0.244 | | 0.359 | 0.055 |
| $R_{X-V}$ | −0.122 | −0.292 | 0.163 | 0.203 | 0.015 | −0.727 | −0.653 | 0.335 | −0.221 | 0.359 | | 0.452 |
| $\Gamma^{\mathrm{G}}$ | −0.256 | 0.008 | 0.225 | 0.386 | −0.052 | −0.708 | −0.498 | 0.309 | −0.127 | 0.055 | 0.452 | |
| RQ BLS1s | | | | | | | | | | | | |
| $\alpha_{6-20\,\mathrm{cm}}$ | | 0.032 | 0.050 | 0.073 | −0.021 | 0.037 | −0.250 | 0.126 | −0.035 | −0.262 | −0.060 | 0.044 |
| $R_{60-25}$ | 0.032 | | −0.484 | −0.564 | −0.208 | 0.319 | −0.210 | −0.481 | 0.707 | 0.039 | −0.365 | −0.154 |
| $J-K_s$ | 0.050 | −0.484 | | 0.842 | 0.657 | −0.321 | −0.238 | 0.427 | −0.240 | −0.080 | 0.069 | 0.226 |
| $H-K_s$ | 0.073 | −0.564 | 0.842 | | 0.212 | −0.459 | −0.024 | 0.411 | −0.284 | −0.003 | 0.146 | 0.284 |
| $J-H$ | −0.021 | −0.208 | 0.657 | 0.212 | | 0.032 | −0.690 | 0.247 | −0.138 | −0.122 | −0.051 | 0.047 |
| $B-V$ | 0.037 | 0.319 | −0.321 | −0.459 | 0.032 | | 0.297 | −0.366 | 0.356 | −0.049 | −0.308 | −0.397 |
| $U-B$ | −0.250 | −0.210 | −0.238 | −0.024 | −0.690 | 0.297 | | −0.273 | 0.279 | −0.054 | −0.451 | −0.338 |
| $B-K_s$ | 0.126 | −0.481 | 0.427 | 0.411 | 0.247 | −0.366 | −0.273 | | −0.034 | 0.250 | 0.206 | 0.213 |
| $R_{60-K_s}$ | −0.035 | 0.707 | −0.240 | −0.284 | −0.138 | 0.356 | 0.279 | −0.034 | | 0.160 | −0.162 | 0.096 |
| $R_{\mathrm{eff}}$ | −0.262 | 0.039 | −0.080 | −0.003 | −0.122 | −0.049 | −0.054 | 0.250 | 0.160 | | 0.345 | −0.048 |
| $R_{X-V}$ | −0.060 | −0.365 | 0.069 | 0.146 | −0.051 | −0.308 | −0.451 | 0.206 | −0.162 | 0.345 | | 0.292 |
| $\Gamma^{\mathrm{G}}$ | 0.044 | −0.154 | 0.226 | 0.284 | 0.047 | −0.397 | −0.338 | 0.213 | 0.096 | −0.048 | 0.292 | |
| RL BLS1s | | | | | | | | | | | | |
| $\alpha_{6-20\,\mathrm{cm}}$ | | 0.554 | −0.151 | −0.125 | −0.099 | −0.163 | −1.000 | −0.099 | 0.152 | 0.461 | −0.004 | 0.224 |
| $R_{60-25}$ | 0.554 | | −0.533 | −0.483 | −0.233 | −0.700 | | −0.100 | 0.933 | −0.132 | 0.857 | 0.709 |
| $J-K_s$ | −0.151 | −0.533 | | 0.795 | 0.772 | 0.307 | | 0.348 | −0.433 | −0.234 | 0.304 | 0.168 |
| $H-K_s$ | −0.125 | −0.483 | 0.795 | | 0.289 | 0.151 | | 0.224 | −0.477 | −0.193 | 0.198 | 0.295 |
| $J-H$ | −0.099 | −0.233 | 0.772 | 0.289 | | 0.344 | | 0.304 | −0.156 | −0.186 | 0.278 | −0.039 |
| $B-V$ | −0.163 | −0.700 | 0.307 | 0.151 | 0.344 | | −1.000 | 0.150 | −0.464 | −0.036 | −0.023 | −0.514 |
| $U-B$ | −1.000 | | | | | −1.000 | | 0.227 | 0.071 | 0.027 | 0.051 | −0.372 |
| $B-K_s$ | −0.099 | −0.100 | 0.348 | 0.224 | 0.304 | 0.150 | 0.227 | | −0.188 | 0.029 | 0.404 | 0.157 |
| $R_{60-K_s}$ | 0.152 | 0.933 | −0.433 | −0.477 | −0.156 | −0.464 | 0.071 | −0.188 | | −0.169 | 1.000 | 0.143 |
| $R_{\mathrm{eff}}$ | 0.461 | −0.132 | −0.234 | −0.193 | −0.186 | −0.036 | 0.027 | 0.029 | −0.169 | | 0.078 | −0.019 |
| $R_{X-V}$ | −0.004 | 0.857 | 0.304 | 0.198 | 0.278 | −0.023 | 0.051 | 0.404 | 1.000 | 0.078 | | 0.219 |
| $\Gamma^{\mathrm{G}}$ | 0.224 | 0.709 | 0.168 | 0.295 | −0.039 | −0.514 | −0.372 | 0.157 | 0.143 | −0.019 | 0.219 | |

## 4 DISCUSSION AND CONCLUSIONS

We have studied broad band properties of NLS1s and a comparison is also made with samples of BLS1 with similar distribution of optical magnitude and redshift. We find that the fraction of RL NLS1s is about 6%, significantly less than that of BLS1s ($\sim 12.6\%$). RL NLS1s are indeed very rare. Five new radio loud NLS1s are found and five RL NLS1 candidates are presented. Distribution of radio loudness of NLS1 is also significantly different as compared with BLS1s in the way that there lacks radio-very-loud sources in the former, while the latter seems to show bimodal distribution with the radio loud peak at $R_{\mathrm{eff}} = 2.75$. We find that the

radio loudness and optical to infrared color $B-K$ are well correlated for RQ BLS1 and NLS1. A radio loud population appears only at $B-K>1.0$ well above the extension of relation defined by radio quiet ones, but formally radio loud NLS1s, as well as a number of other RL BLS1s, are on this extension.

It was found that two RL NLS1 (2E 1640+5345 and RXS J16290+4007) have inverted radio spectral indexes, another RL NLS1, RXS J16333+4718, has flat radio spectrum, while other five RL NLS1s with multiple radio band observations (listed in Table 4) are steep radio sources. It is clearly that the radio spectra of RL NLS1s can be either steep or flat. Note that these three flat spectra sources are among the powerful RL NLS1s ($P_{6\,\mathrm{cm}}>10^{24.5}$ W Hz$^{-1}$). It is worthy to notice that HE 0132−4313 and PKS 0558−504 are also very powerful radio source, though they were not covered by either FIRST or NVSS, but their radio spectrum is quite steep ($\alpha_{3.6-6\,\mathrm{cm}}=1.4$ and $\alpha_{2.7-4.85\,\mathrm{GHz}}=0.6$). The radio structure of He 0132–4313 is unresolved in the high resolution VLA image (Grupe et al. 2000), while no high resolution radio observation has been made for PKS 0558–504. It will be interesting to see if these two sources are compact steep spectrum (CSS) radio sources, which were considered as young radio sources (Gelderman 1997). Alternatively, as Grupe et al. (2000) noted, the flat radio spectrum in HE 0132 could be due to the variability of the source and the spectral index was derived from non-simultaneous observations. If this is indeed the case, then most powerful radio loud NLS1s will tend to have flat radio spectra. While most radio quiet ones with steep radio spectra. The latter is consistent with the result of Moran (2000).

These results are qualitatively consistent with the picture that NLS1s possess low mass black holes and high accretion rate in general. The lack of radio-very-loud objects in the NLS1 sample implies that no NLS1 contains very massive black hole. Using empirical relation of Broad Line Region (BLR) size with luminosity and virialization assumption, Wang et al. (2001) pointed out that RL NLS1s have low BH masses. Furthermore, Ho (2002) found that Radio-loudness $R$ is strongly inversely correlated with the ratio of nuclear luminosity to the Eddington luminosity $L/L_{\mathrm{E}}$, and hence with mass accretion rate, i.e., it is reasonable that RL NLS1s are very rare because of high accretion rate for most NLS1s. This anti-correlation of $R$ and $L/L_{\mathrm{E}}$ would be useful to explain the lack of radio-very-loud NLS1s and consequently the low fraction of RL NLS1s. However, there are increasing evidences that strong radio emission is associated with large black hole mass (Laor 2000; Dunlop & McLure 2000; Lacy et al. 2001). In the sample of Laor (2000), all the RL AGNs possess central BHs with $M_{\mathrm{BH}}>6\times10^{8}M_{\odot}$. Nevertheless, the radio loudness of RL NLS1s is only moderate. PKS 2004–447 is an exception, but this object does not show FeII emission (Osblak, Webster & Whitins 2001). If the radio emission has been boosted relativistically in RL NLS1s, then the intrinsic radio loudness need not to be large. Apparently , flat radio spectra of some RL NLS1s suggest that this maybe the case. The presence of rapid flare in PKS 0558−504 is viewed as evidence of relativistic beaming in this object (Remillard et al. 1992) although there are other possibilities (Wang et al. 2001).

It was also found that the radio power is well correlated with central black hole mass for radio quiet objects, but radio loud objects apparently have higher radio power than this relation (Nelson 2001). If this is also valid for NLS1, then the similar distributions of radio loudness and radio power for BLS1 and NLS1 at the radio weak/intermediate portion suggest that BH mass distributions for radio-quiet BLS1 and NLS1 are similar. This contradicts the previous interpretation that NLS1 possess low mass black holes. So we are in a dilemma that either radio power-BH mass correlation is broken down for NLS1s or NLS1s do not possess small BH mass. While the former relation should be tested further, firm evidence for small BH masses is

still lacking.

One argument for the low BH mass is the narrow H$\beta$ line width. Reverberation mapping shows that BLR in Seyfert galaxies is virialized, and the line emission region is approximately scaled with luminosity according to $L^{0.5-0.7}$ (e.g., Wandel et al. 1999; Kaspi et al. 2000). If these results are also valid for NLS1s, then low BH masses are obtained for NLS1s with additional assumption that the velocity distribution of BLR is close to isotropic. With these masses, NLS1s is emitting at a significant fraction of Eddington luminosity. The radiation force on the BLR clouds can be comparable to or even larger than the gravitational force of the central BH, since the line absorption opacity can be considerably larger than Thomson scattering one. Then the internal consistency of these assumptions is questionable. If virialization is applicable to the H$\beta$ line emitting clouds, one has to assume that the line clouds see considerably weaker continuum than we do, and quasi-steady static assumption also means that the velocity of clouds must be isotropic. The former one tends to overestimate the size of BLR, hence the BH mass, while the latter one will tend to underestimate the true velocity dispersion of BLR. Whether the two can cancel each other depends on the isotropic pattern of continuum and the velocity field.

A second line of evidence for low BH mass comes from the rapid variability of the X-ray flux. Boller et al. (1996) noticed that NLS1s are systematically more variable than BLS1s. A quantitative study by using ASCA database suggested that NLS1s show systematically larger variability amplitude than BLS1s (Leighly 1999). Although this result does not obviously imply low mass BH in NLS1s, compelling evidence for a good correlation between X-ray variability and the BH mass derived from reverberation mapping was found by Lu & Yu (2001) for a sample of Seyfert 1 galaxies, including three NLS1s. Again, we do not know if virialization assumption is applicable to NLS1s, i.e., the kinematic mass from reverberation mapping is correct. However, we note that the mass derived from reverberation mapping agrees with that from empirical relation between the galaxy bulge velocity dispersion and BH mass for a dozen BLS1s and NLS1s (Ferrarese 2001; Wang & Lu 2001). This implies that the anisotropic effect must have been canceled by other effects.

Another widely debated issue is whether radio emission in RL and RQ objects is physically the same and the only difference is the energy output in the radio jets. We found clear different behavior of radio loud and radio quiet sources in various diagrams: nucleus power versus optical/NIR colors, X-ray luminosity versus X-ray spectral index, optical color versus NIR colors, and also various luminosity-luminosity correlations. In particular, the radio power is only very loosely correlated with soft X-ray luminosity, but moderately strong with far-infrared luminosity for RQ BLS1s and NLS1s. On the contrary, the radio power correlates much more tightly with soft X-ray luminosity, and not with far-infrared luminosity for RL BLS1s. This suggests that radio emission detected by NVSS and FIRST in RQ BLS1s and NLS1s connects poorly with the nucleus power. There are three possibilities for this: contamination of extended radio emission from host galaxies, large variation of nucleus power during the expansion of radio jet, dependence of radio power on many other parameters, which vary from objects to objects. It seems that the first possibility is more likely, as the radio to far-infrared ratio is similar to that of normal and starburst galaxies. However, high resolution radio data are required to distinguish these possibilities.

Radio loud Seyfert 1 galaxies are found to have bluer optical color ($B-R$) than radio quiet ones. One possibility is due to the contribution of the jets, which usually have flat spectrum. Another possible explanation might be that the relative contributions of stellar and nuclear

components of the two are different. The nuclei of radio loud sources as a whole are more powerful than radio quiet ones and the optical spectrum of nucleus is harder than that of the host galaxy.

We have tentative result that NLS1s are relatively brighter in mid/far-infrared band than BLS1s, and NLS1s also show larger $J - K$ ($K$-excess) than BLS1s. If the accretion rate of NLS1s is much higher than BLS1s, there would be more fueling gas near the central engine. Therefore we would expect that NLS1s locate at dust-richer environment.

NLS1s usually have steep soft X-ray spectrum, but a significant fraction of them shows flat spectra. We find that most X-ray flat spectrum sources either display strong absorption or large variation in the X-ray spectrum. We also find that the X-ray spectral index is anti-correlated with the optical colors. Hence, our result tends to suggest that most NLS1s should have intrinsically steep X-ray spectrum if there is no absorption.

**Acknowledgements** We thank Dr. Weimin Yuan for helping with the ROSAT data analysis and Dr. Youjun Lu for critically reading of an early version of this paper. We also thank the referee for useful comments. This work is supported by the National Natural Science Foundation of China and a key program of Chinese Science and Technology ministry. This work has made use of NED, and data products from the Two Micron All Sky Survey, which is a joint project of the University of Massachusetts and the Infrared Processing and Analysis Center/California Institute of Technology, funded by the National Aeronautics and Space Administration and the National Science Foundation.

## References

Aoki K., Yoshida M., 1999, In: G. Ferland, J. Baldwin, eds., Quasars and Cosmology, ASP: San Francisco, p.385
Boller Th., Brandt W. N., Fink H., 1996, A&A, 305, 53
Bonatto C. J., Pastoriza M. G., 1997, ApJ, 486, 132
Boroson T. A., Green R. F., 1992, ApJS, 80, 109
Brinkmann W., Yuan W., Siebert J., 1997, A&A, 319, 413
Dunlop J. S., McLure R. J., Kukula M. J., 2000, MNRAS, 318, 693
Ferrarese L., Pogge R., Peterson B. M., Merritt D., Wandel A., Joseph C. L., 2001, ApJ, 555, L79
Gelderman R., 1997, American Astronomical Society Meeting, 191, 2202
Gliozzi M., Boller Th., Brinkmann W., Brandt W. N., 2000, A&A, 356, L17
Grupe A. et al., 1999, A&A, 350, 805
Grupe A., Leighly K., Thomas H. C., Laurent-Muehleisen S. A., 2000, A&A, 356, 11
Ho L. C., ApJ, 564, 120
Kaspi S., Smith P. S., Netzer H., Maoz D., Jannuzi B. T., Giveon U., 2000, ApJ, 533, 631
Lacy M., Laurent-Muehleisen S. A., Ridgway S. E., Becker R. H., White R. L., 2001, ApJ, 551, 17L
Laor A., Fiore F., Elvis M., Wilkes B. J., McDowell J. C., 1994, ApJ, 435, 611
Laor A., Fiore F., Elvis M., Wilkes B. J., McDowell J. C., 1997, ApJ, 477, 93
Laor A., 2000, ApJ, 543, L111
Lawson A. J., Turner M. J. L., 1997, MNRAS, 288, 920
Leighly K., 1999, ApJS, 125, 317
Lu Y. J., Yu Q. J., 2001, MNRAS, 324, 653
Marziani P., Sulentic J. W., Zwitter T., Dultzin-Hacyan D., Calvani M., 2001, ApJ, 558, 553
Moshir M., 1989, IRAS Faint Source Survey, (IPAC: Pasedena)

Moran E. C., 2000, New Astronomy Review, 44, 527
Nelson C. H., 2000, ApJ, 544, L91
Pogge R. W., 2000, New Astronomy Reviews, 44, 381
Puchnarewicz E. M., Branduardi-Raymont G., Mason K. O., Sekiguchi K., 1995, MNRAS, 276, 1281
Remillard R. A., Grossan B., Bradt H. V., Ohashi T., Hayashida K., Makino F., Tanaka Y., 1992, Nature, 350, 589
Schartel N., Walter R., Fink H. H., Truemper J., 1996, A&A, 307, 33
Siebert J., Leighly K. M., Laurent-Muehleisen S. A., Brinkmann W. et al., 1999, A&A, 348, 678
Skrutskie M. F., Schneider S. E., Stiening R. et al., 1997, In: F. Garzon, et al., eds., The Impact of Large Scale Near-IR Sky Surveys, Dordrecht: Kluwer, p.25
Sulentic J. W., Zwitter T., Marziani I. P., Dultzin-Hacyan D., 2000, 536, L5
Véron-Cetty M. P., Véron P., Goncalves A. C., 2001, A&A, 372, 730
Véron_Cetty M. P., Véron P., 2001, A&A, 374, 92
Voges W., Aschenbach B., Boller Th. et al., 1999, A&A, 349, 389
Voges W., 1997, Data Analysis in Astronomy IV, 189
Wang T., Brinkmann W., Bergeron J., 1996, A&A, 309, 81
Wang T. G., Lu Y. J., 2001, A&A, 377, 52
Wang T. G., Matsuoka M., Kubo H., Mihara T., Negoro H., 2001, ApJ, 554, 233
Walter R., Fink H. H., 1993, A&A, 274, 105
Wills B. J., Laor A., Brotherton M. S., Wills D., Wilkes B. J., Ferland G. J., Shang Z., 1999, ApJ, 515, L53
Yuan W., Brinkmann W., Siebert J., Voges W., 1998, A&A, 330, 108